Journal of Sound and Vibration (1999) **222**(4), 635–668
Article No. jsvi.1998.2094, available online at http://www.idealibrary.com on IDEAL

ACTIVE CONTROL OF ENVIRONMENTAL NOISE, IV: PRACTICAL EXTENSIONS TO ECAS THEORY

S. E. WRIGHT AND B. VUKSANOVIC
*School of Engineering, University of Huddersfield, Huddersfield HD*1 3*DH, England*

(*Received* 16 *March* 1998, *and in final form* 17 *December* 1998)

The basic Electronically Controlled Acoustic Shadow (ECAS) model in Paper I [1] (Wright and Vuksanovic 1996 *Journal of Sound and Vibration* **190**, 565–585), considered the sound cancellation from a flat (2D), in-phase primary source, radiating in free field (no reflecting surfaces) and in a stationary propagating fluid (no wind), using monopole (omnidirection) cancellers. In Paper II [2] (Wright and Vuksanovic 1997 *Journal of Sound and Vibration* **202**, 313–359), the theory was extended to high frequency non-compact acoustic sources, where the acoustic wavelength is small compared to the source size. Paper III [3] (Wright and Vuksanovic 1999 *Journal of Sound and Vibration*, **220**, 469–496) considered the implementation of ECAS theory into practice. This paper considers the following practical extensions to the basic ECAS model: (a) out-of-phase primary sources; (b) three-dimensional primary sources; (c) ground reflection; (d) directional secondary sources and (e) wind effect.

1. INTRODUCTION

The detailed properties of the basic ECAS system, illustrated in Figure 1, are given in references [1–3]. For comparison with the following model extensions, the unit shadow $\alpha = \beta = 15°$ is used. Here the sound is generated by a square, in-phase primary source plane, of dimensions $D = 2$ m and total source strength $Q_p = 1$ m^3/s. Point sources used in the primary array are identical and equispaced, with strengths $q_p = Q_p/p$, where p is the number of sources in the array; i.e., for $p = 16$, $q_p = 1/16$ m^3/s $= 0{\cdot}063$ m^3/s. An array of 3×3 secondary (cancelling) sources lie in a plane, with the sources separated from each other by $d = 1$ m; the distance of this plane from the primary source plane is $r_s = \lambda/2 = 1{\cdot}715$ m for 100 Hz and $\lambda/2 = 0{\cdot}429$ m for 400 Hz source frequency. λ is the acoustic wavelength.

A corresponding 3×3 microphone array is situated at $r_m = 50$ m from the primary source, within the $15 \times 15°$ control angles. Figures 2(a) and (b) show the uncancelled (dotted line) and cancelled (full line) $60° \times 360°$ observer strip, situated at an observer distance of $r_0 = 50$ m around the source. These figures are computed for a 100-Hz, compact primary source (dimensions $D > \lambda$) and for a 400-Hz non-compact source ($D > \lambda$). Note that the 400-Hz source is approximately four times (12 dB) higher than the 100-Hz source for the same source strength.

0022–460X/99/190635 + 34 $30.00/0

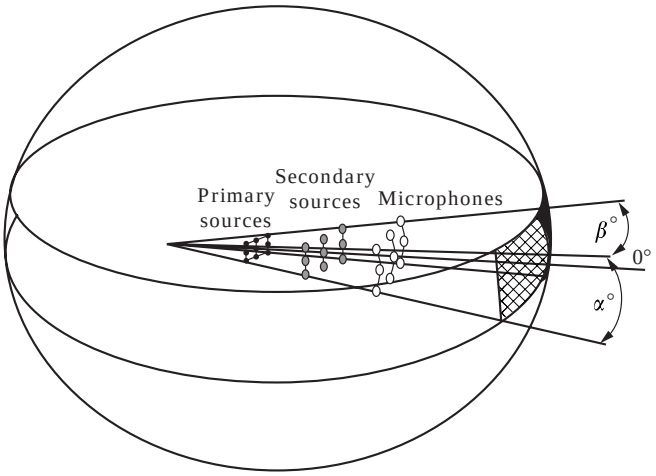

Figure 1. Electronically Controlled Acoustic Shadow (ECAS) system.

Equations (1) predict the average shadow depth for the $15 \times 15°$ unit shadow, for an observer $\gg$ microphone $\gg$ secondary source distance from the primary source; the shadow depth for a compact source is given by the first equation and for a non-compact source by the second equation; here n is 10, 13 and 16 for primary–secondary source plane separation distances r_s of 2λ, $\lambda/2$ and $\lambda/8$ respectively:

$$\text{dB} \cong 10n \log(\lambda/d), \quad D < \lambda; \qquad \text{dB} \cong n \log 2(\lambda/d), \quad D > \lambda. \tag{1}$$

As the shadow depth in dB and the shadow angle in degrees are approximately linear with the number of channels, the channel number for larger shadows can be estimated by the addition of these $15 \times 15°$ unit shadows. The theory thus predicts deep shadows for large sources at low frequencies, or small sources at high frequencies; or large shadow angles for compact sources, or small shadow angles for non-compact sources, for the same channel number. For example, if $\lambda/d = 2$ and $n = 13$, the shadow depth would be ≈ 39 dB for $D < \lambda$. If the source frequency $f = 100$ Hz, $\lambda = 3{\cdot}4$ m, and $d = 1{\cdot}7$ m, then if $D \cong 3{\cdot}4$ m, the number of secondary cancellers per source dimension $N \approx (D/d + 1) \approx 3$ or 9 for a square source over $15° \times 15°$, or 15 cancellers over $15° \times 30°$.

2. OUT-OF-PHASE PRIMARY SOURCES

The primary source in the basic ANC model was treated as a two-dimensional array of point sources, vibrating in phase and with the same amplitude and frequency. In the case of real primary systems, this model is an over-simplification. Mechanical structures will have higher order modes. It is important to establish the effect on shadow depth from these higher order modes compared with the simple in-phase sources. These modes can be obtained by solving the wave equation for the primary structure with appropriately chosen boundary conditions. A two-dimensional version of the wave equation, where $y = y(x, z, t)$ represents the transverse displacement of a flat structure, can be expressed as

$$\partial^2 y/\partial x^2 + \partial^2 y/\partial z^2 = (1/c^2)\partial^2 y/\partial t^2. \tag{2}$$

The well known solution of this wave equation, given for example, in reference [4], upon neglecting the time variation factor is

$$y(x, z) = A \sin k_x x \sin k_z z, \tag{3}$$

$$k_x = n\pi/w_p, \quad n = 1, 2, 3, \ldots, \qquad k_z = m\pi/b_p, \quad m = 1, 2, 3, \ldots. \tag{3a, b}$$

(a)

System parameters: P=6×6, S=3×3, M=3×3, f=100 Hz, λ=3.43 m, D=2 m, λ/D=1.7, r_s=1.71 m, (λ/D), r_M=r_0=50 m; shadow angles: α_{sh}=15° (azimuth), β_{sh}=15° (elevation)

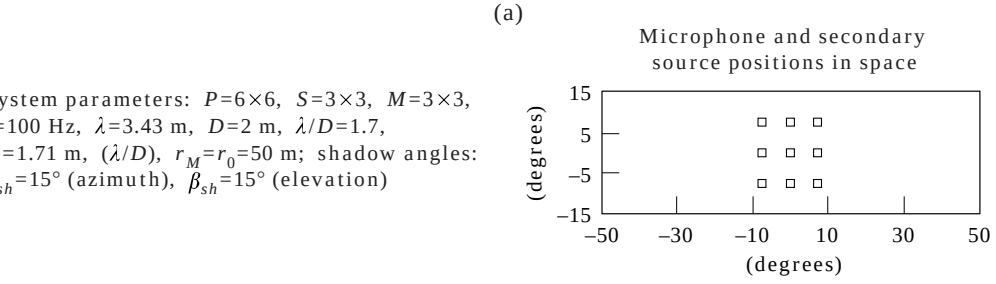

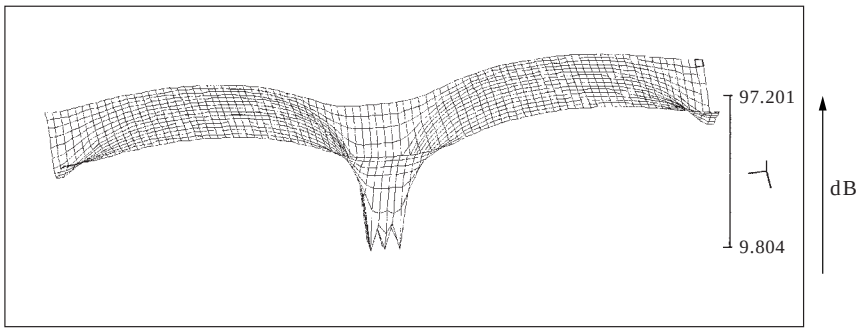

Γ

dB relief

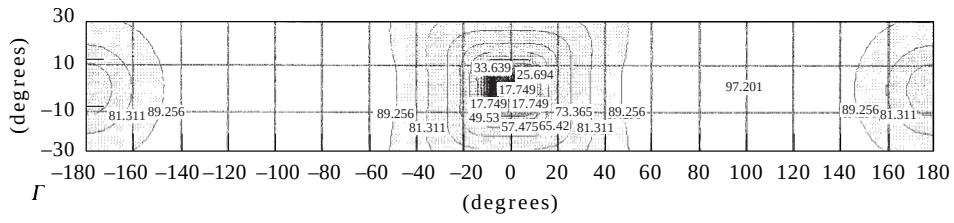

Γ

dB contours

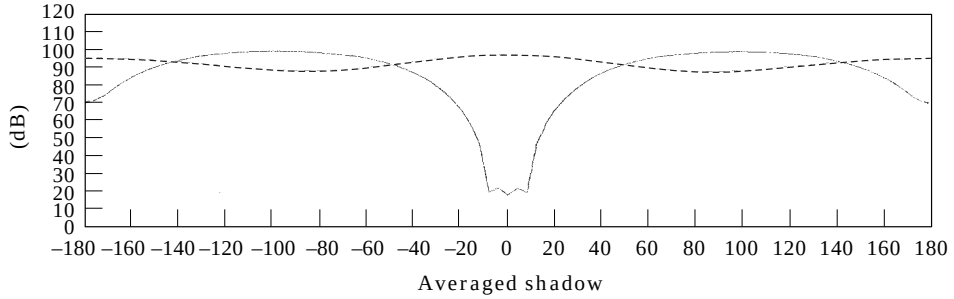

Averaged shadow

Figure 2(a) *Caption overleaf*

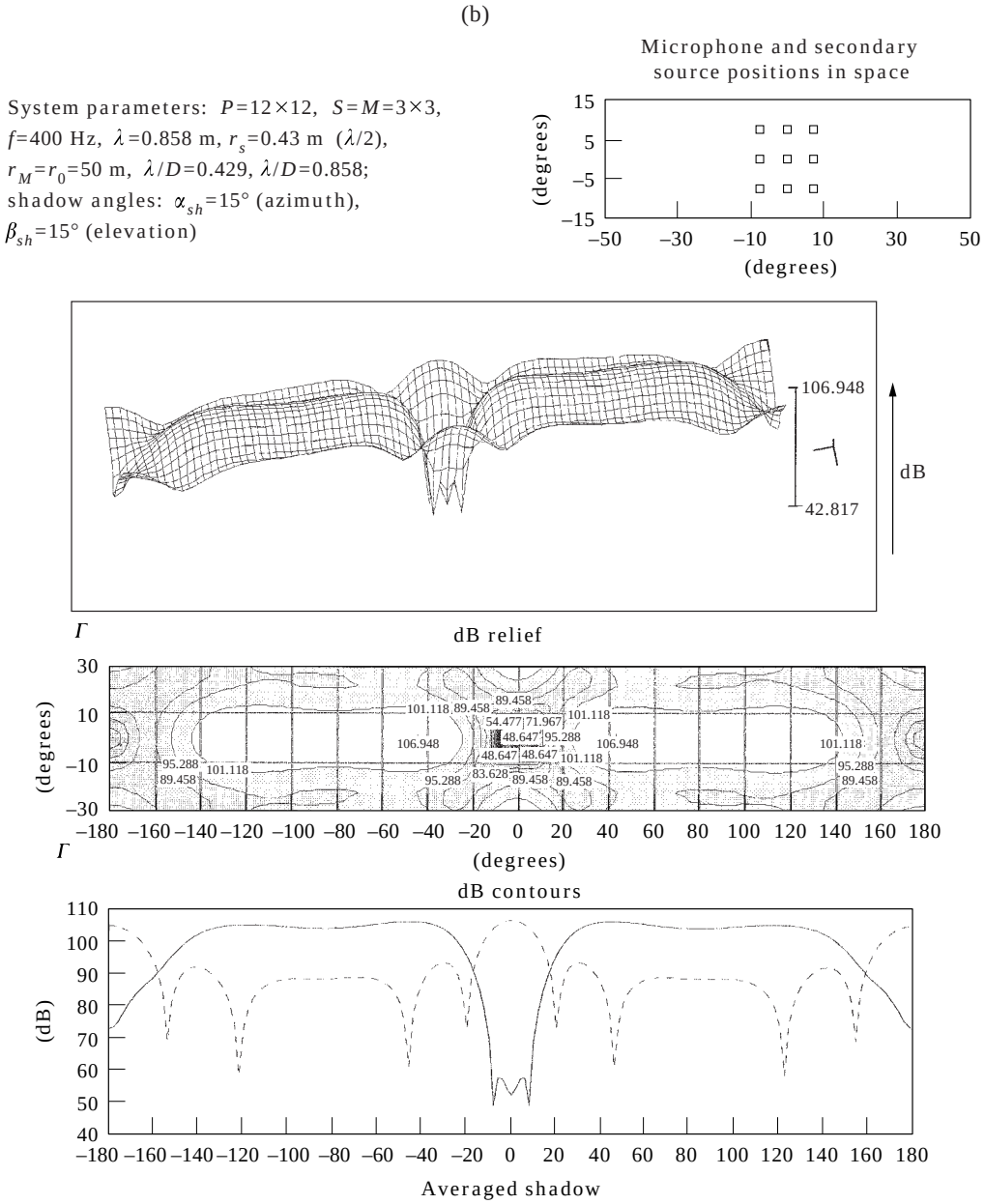

Figure 2. (a) $15\times15°$ unit shadow, $f=100$ Hz. (b) $15\times15°$ unit shadow, $f=400$ Hz.

Here w and b are the width and breadth of the plate. The first order mode and a few of the higher order modes, given by equations (3), are shown in Figure 3. Each of the modes is denoted by an index (n, m). The modes are simulated, approximately, by point sources; the positive sources are denoted by open circles and the negative sources (out of phase by 180°) by filled circles.

Figure 4 shows the intricate beauty of the sound pressure contours in dB, of a $\pm60°$ elevation by $\pm180°$ azimuth observer strip situated at 50 m around the source.

Various vibration modes, from a 2-m square source radiating at 100 and 400 Hz source frequencies are considered. The individual strength of each point source is set at $q_p = 1/p$ m^3/s (where $p = 16$ is the number of sources in the primary array).

Mode (a) in Figure 4(a) is basically the directivity of a marginally compact monopole source for an acoustic frequency $f = 100$ Hz ($\lambda/D = 1{\cdot}7$). It has a maximum radiation at the front (0°) and back (180°) of the source, and slightly reduced radiation in the plane of the source (90°), through destructive interference across the source. Mode (b) is equivalent to a lateral dipole having minimum radiation at 0° and 180° azimuth. Modes (c) and (d) are basically

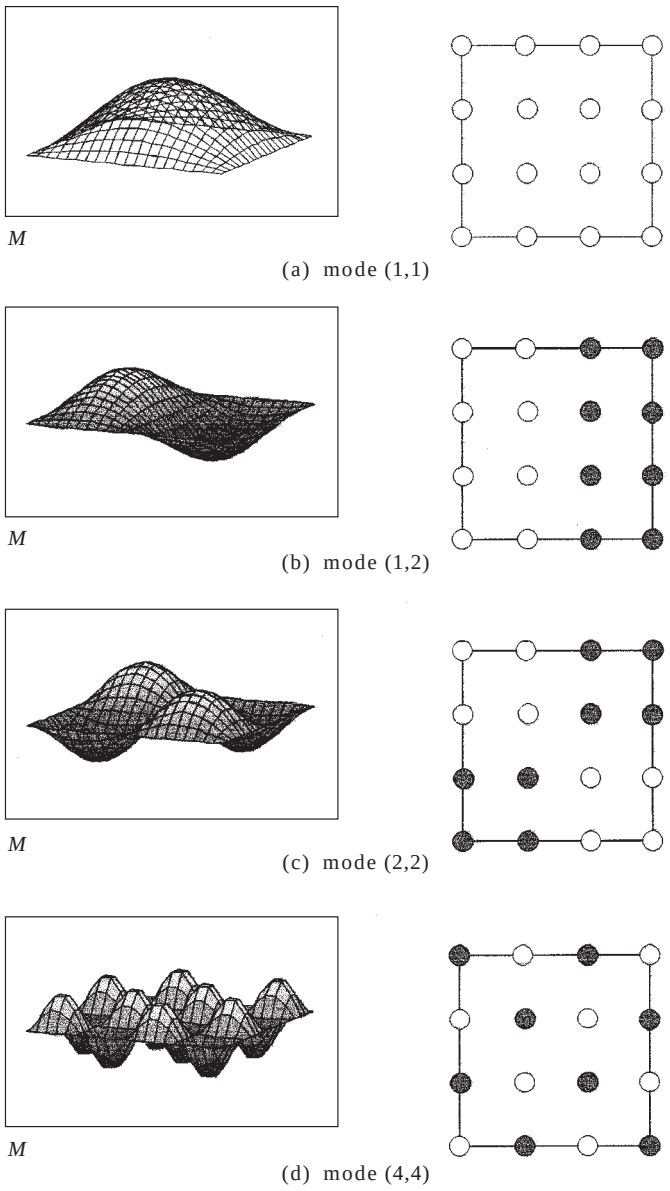

Figure 3. Some of the normal vibration modes of the primary sound source.

(a)

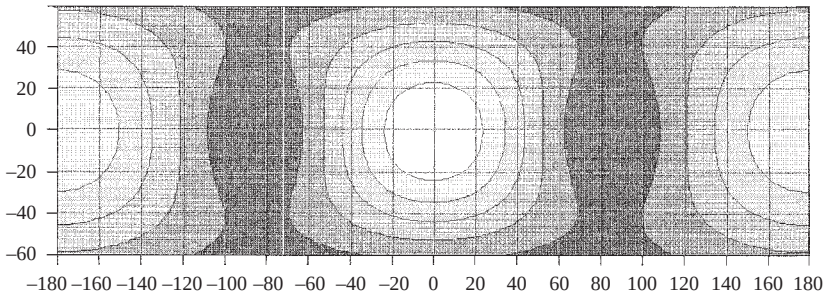

Mode a (1,1)

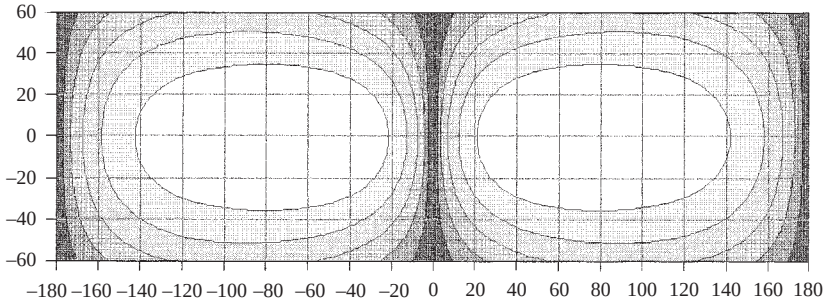

Mode b (1,2)

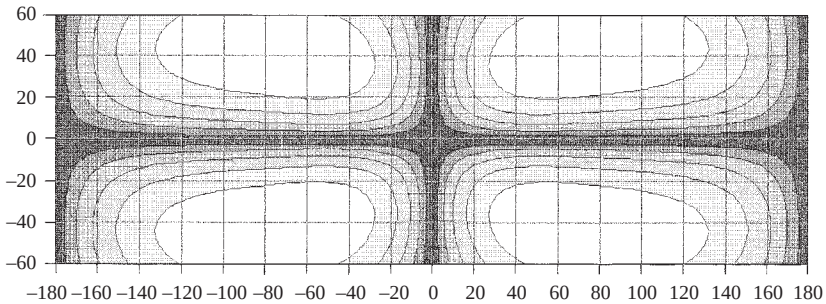

Mode c (2,2)

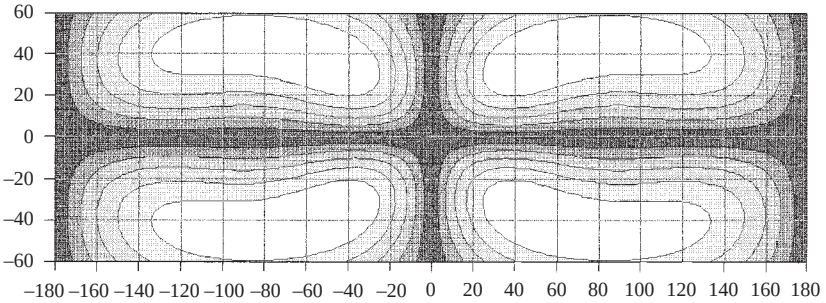

Mode d (4,4)

Figure 4(a) *Caption opposite*

(b)

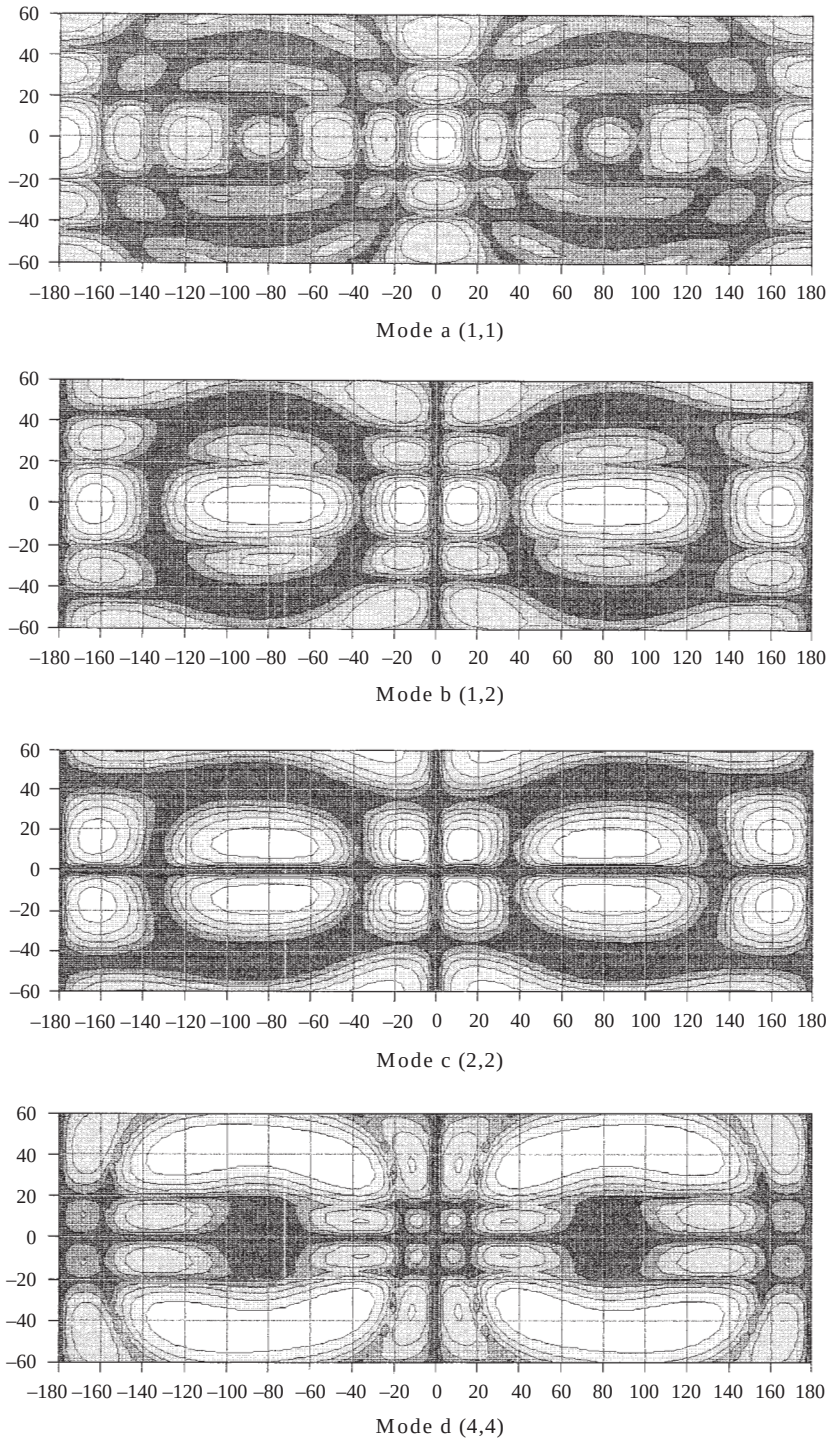

Figure 4. (a) Radiation characteristics of vibration modes, $f = 100$ Hz. (b) Radiation characteristics of vibration modes, $f = 400$ Hz.

lateral quadrupole directivities with minimum radiation at 0° and 180° azimuth. and 0°, 180° elevation angles. In Figure 4(b) modes (a) to (d) give similar multipole directivities for $f = 400$ Hz, showing the additional complex interference, through source non-compactness ($\lambda/D = 0{\cdot}429$).

As to the shadow generation from these modes, Figure 5–8 show the uncancelled (dotted line) and cancelled fields for modes 2,2 and 4,4 for $15 \times 15°$ and $30 \times 15°$ shadows at 100 and 400 Hz. Note that the radiation of the uncancelled out-of-phase sound at low frequencies is ≈ 70 dB compared with the in-phase source level at ≈ 95 dB, shown in Figure 2(a), a difference of 25 dB.

At 100 Hz, shown in Figures 5 and 6, the shadow depth for mode 2,2 (and mode 4,4 not shown), is approximately 50 dB $(75 - 25)$ compared to ~ 75 dB $(95 - 20)$ for the in-phase source mode, given in Figure 2(a)—a loss of shadow depth of ~ 25 dB. At 400 Hz, shown in Figures 7 and 8, both mode 2,2 and mode 4,4 give ~ 30 dB $(95 - 65)$ shadows, compared with ~ 50 dB $(105 - 55)$, for the in-phase source in Figure 2(b)—a loss of ~ 20 dB.

In summary, it can be seen that there is aproximately 25 and 20 dB shadow loss for compact and non-compact out-of-phase sources, respectively, compared with the in-phase case. Although the radiation fields from the higher order modes are complex, having wave fronts with phase reversals, deep shadows are still formed across them.

3. THREE-DIMENSIONAL PRIMARY SOURCES

A second extension to the simple 2D flat primary source of the basic ECAS model is the effect of source depth. Three primary source configurations considered are (a) front and top surface, Figures 9 and 11, (b) front and side, Figures 10 and 12, and (c) a corner (not shown) of a 2-m cube, for 100 and 400 Hz source frequencies. The number of primary sources used in constructing

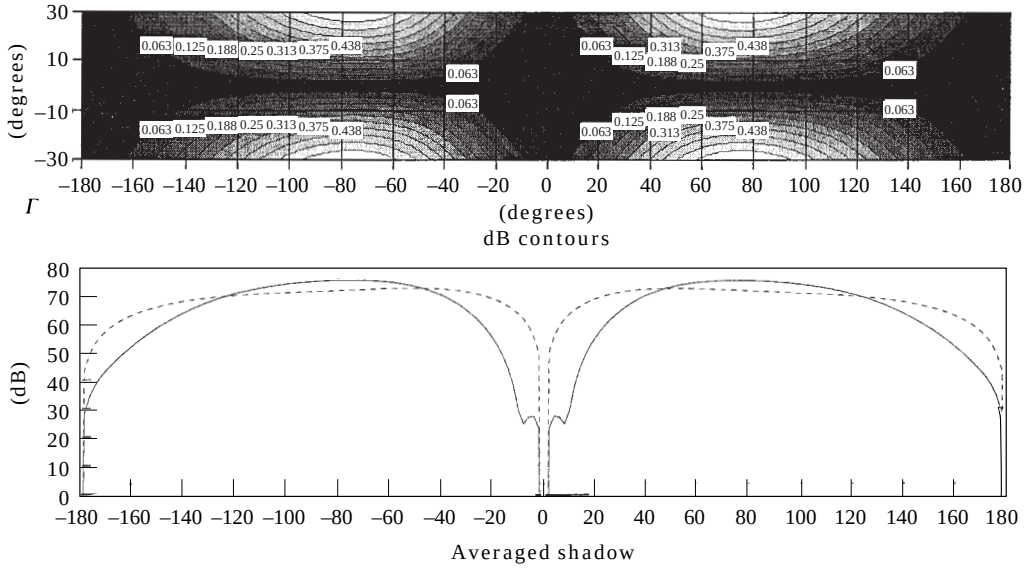

Figure 5. $15 \times 15°$ shadow for out-of-phase primary source, $f = 100$ Hz, mode (2,2).

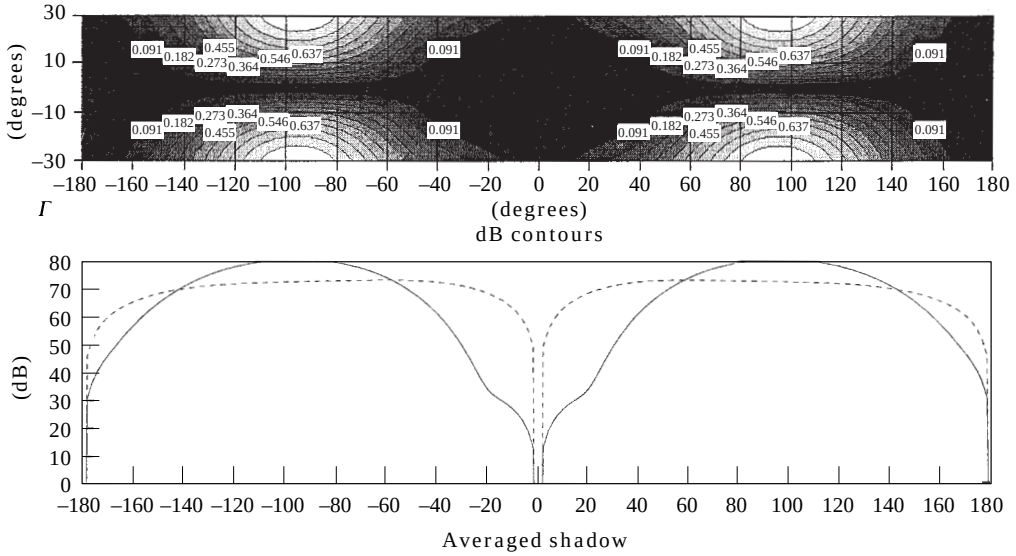

Figure 6. $30 \times 15^\circ$ shadow for out-of-phase primary source, $f = 100$ Hz, mode (2,2).

the 3D primary sources is 5×5 for each source face with corner sources common to both faces, a total source strength of 1 m^3/s, giving $1/45$ m^3/s for each of the $(5 \times 5) + (5 \times 4) = 45$ sources.

It can be seen that the basic effect of a 3D source compared with a 2D source, as to be expected, is to produce a more spherical-like radiation directivity: i.e., to increase the side radiation facing the additional surface, where the radiation from a 2D flat surface is reduced for a non-compact source. At low frequencies, the compactness is reduced with the extra dimension, reducing the shadow from ~ 75 to ~ 50 dB (25 dB reduction). At high frequencies, the source is already

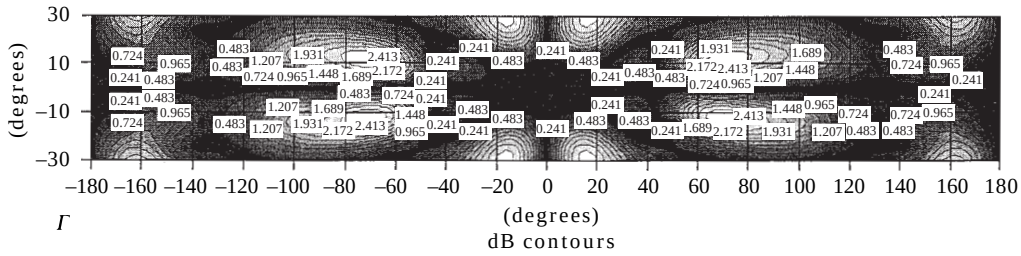

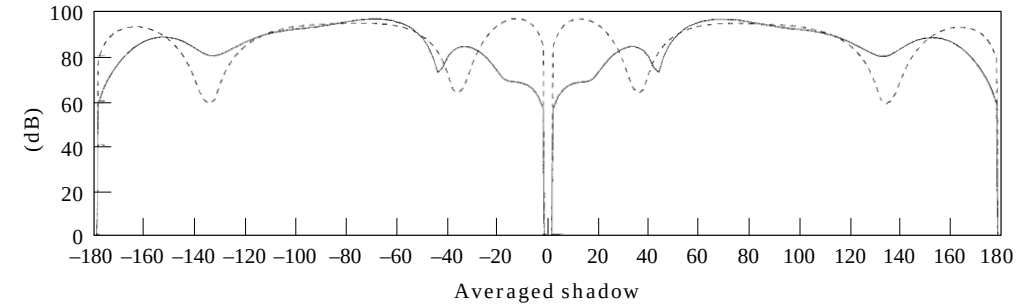

Figure 7. $30 \times 15^\circ$ shadow for out-of-phase primary source, $f = 400$ Hz, mode (2,2).

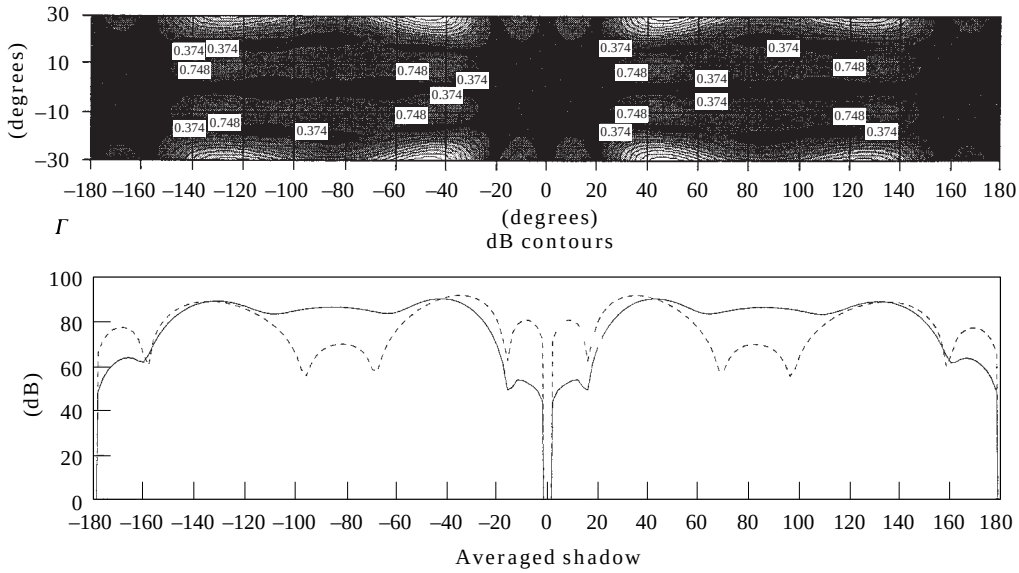

Figure 8. $30 \times 15^{\circ}$ shadow for out-of-phase primary source, $f = 400$ Hz, mode (4,4).

substantially non-compact and the shadow depth is only marginally reduced with the extra dimension, reducing from 50 to 40 dB (10 dB reduction). A corner situation tends to give slightly larger shadow losses.

4. GROUND REFLECTION

A third extension to the basic free field radiation model is the effect of reflecting surfaces, particularly ground reflection. The complex sound pressure

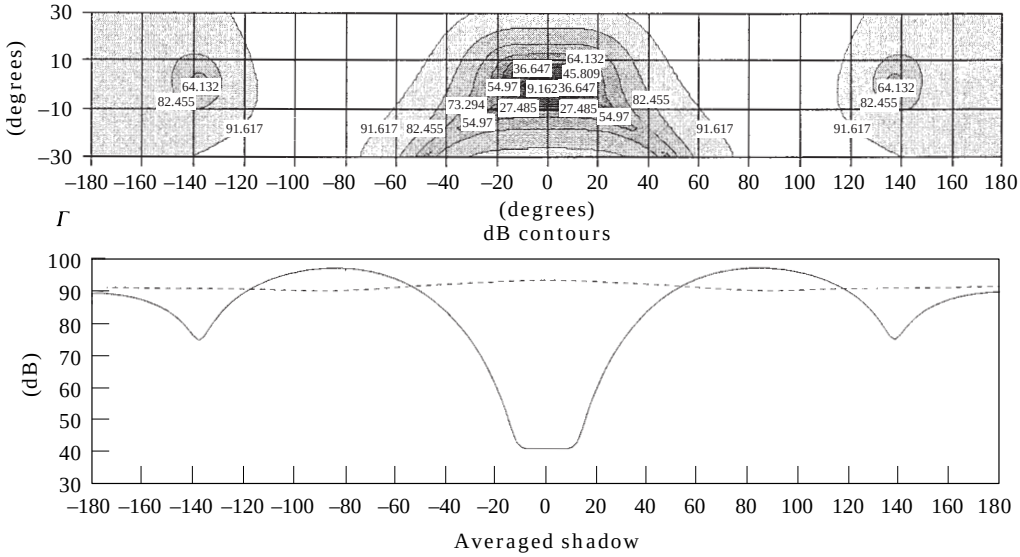

Figure 9. 100-Hz unit shadow for 3D source, front and top.

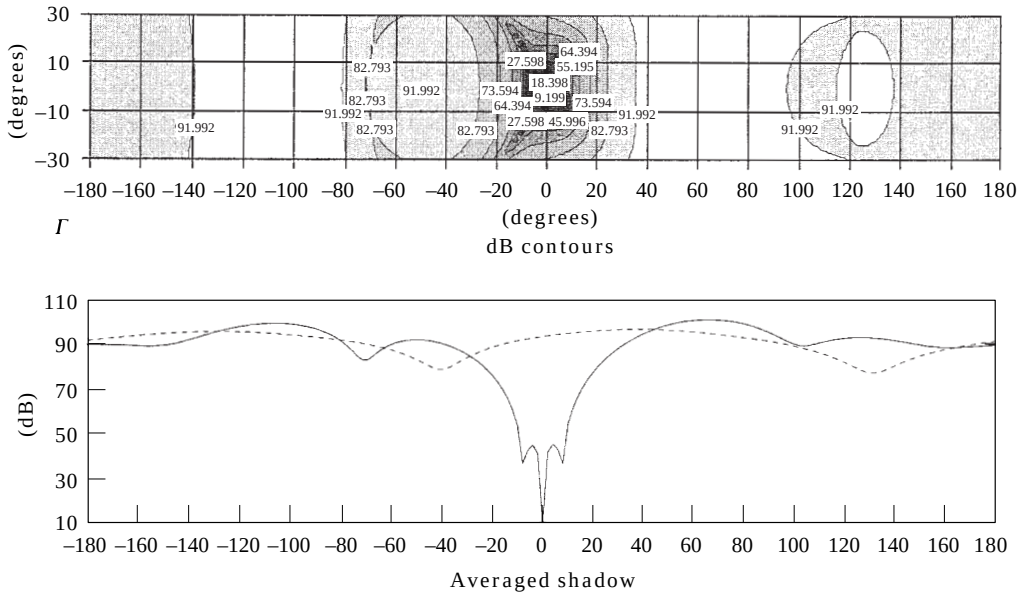

Figure 10. 100-Hz unit shadow for 3D source, front and side.

$p(r)$ in Pascals at some distance r from a single, monopole point sound source S, upon neglecting the harmonic time varing term $\exp(j\omega t)$, can be calculated by using the equation

$$p(r) = c_p(r)q, \tag{4}$$

where the propagation coefficient $c_p(r)$ is

$$c_p(r) = (j\omega\rho_0/4\pi r)\, e^{-jkr}, \tag{5}$$

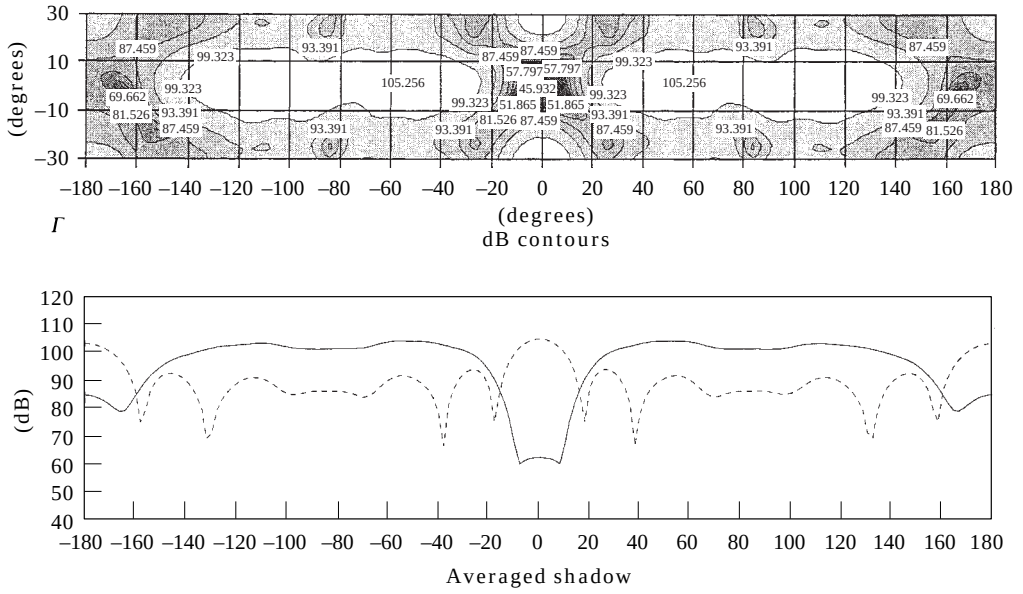

Figure 11. 400-Hz unit shadow for 3D source, front and top.

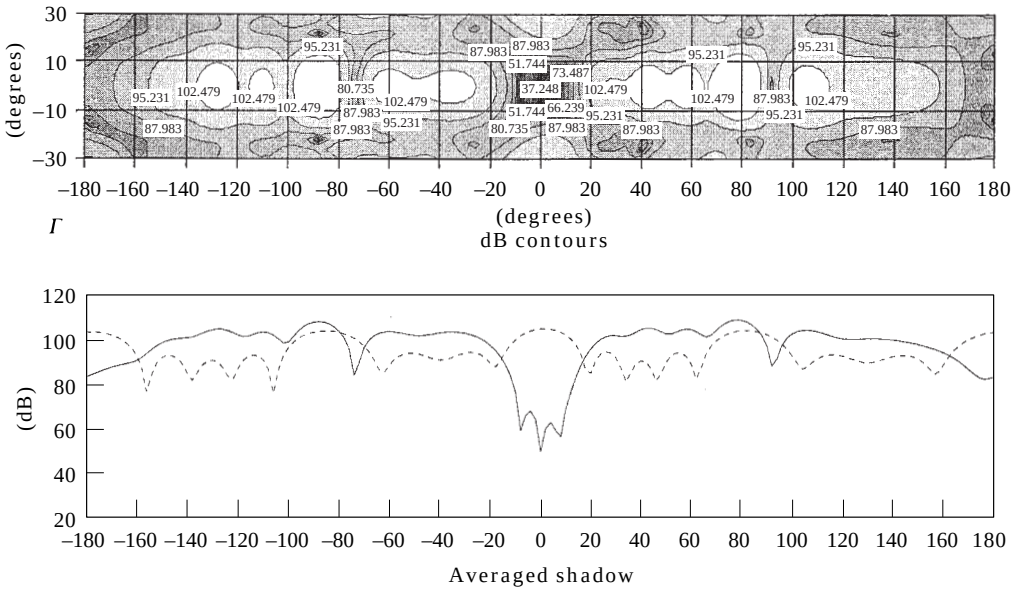

Figure 12. 400-Hz unit shadow for 3D source, front and side.

where $\omega = 2\pi f$ is the angular frequency of the source in rad/s, ρ_0 is the density of the propagating medium (kg/m^3), q is the complex source strength (m^3/s) and k is the wave number (ω/c) where c is the speed of sound.

In the case of a reflective ground surface, sound at the microphone position M will be the sum of the direct and reflected sound. The surface can be replaced by a "mirror image" of point sources of appropriate strength (taking into account the ground reflectivity), positioned at S' as shown in Figure 13. In the case of a 100% reflective surface, using a modified form of equation (4), the complex sound pressure at point M can be calculated as

$$p(r) = (c_p(r) + c_p(r'))q. \tag{6}$$

In a more realistic case of a surface which absorbs partly the sound from a source (grass or some other absorbing material) the above equation can be changed by using an absorption factor α:

$$p(r) = (c_p(r) + \alpha c_p(r'))q. \tag{7}$$

The reflecting surface can also in some cases introduce a change in phase between the incident and reflected sound. Equation (6) can also be changed to accommodate this phase. For 90° phase shift one has

$$p(r) = (c_p(r) + \mathrm{i}\alpha c_p(r'))q, \tag{8}$$

where $\mathrm{i} = (-1)^{1/2}$.

With reference to Figure 14, the sound at each microphone, from the microphone array, can be expressed by using the matrix equation

$$P_m = (C_m + C_{m'})Q_p, \tag{9}$$

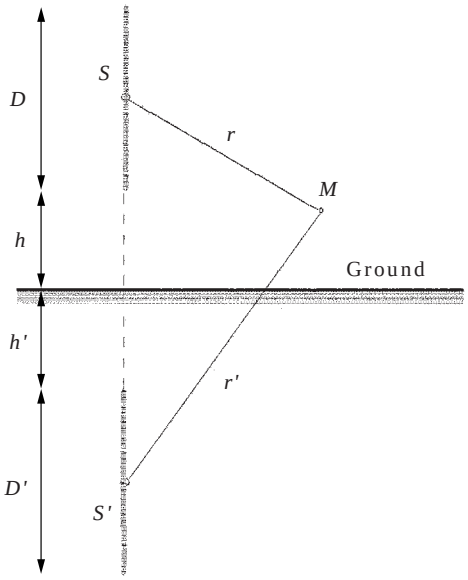

Figure 13. Geometry of sound source, ground reflection image and microphone.

where P_m represents the m-dimensional vector of complex sound pressures at each microphone from the array (m is number of microphones in the microphone array), Q_p is the p-dimensional vector of complex source strengths (p is the number of point primary sources in the array) and C_m, $C_{m'}$ are matrices of propagation coefficients between each point source from real and image arrays, respectively, to each microphone array (dimensions of these matrices are $m \times p$).

Due to the "mirroring effect" of the ground plane, the order of particular columns in the matrix C_m is reversed. For the case of 3×3 source and microphone arrangement in space, the matrix $C_{m'}$ is

$$C_{m'} = \begin{bmatrix} c_{0\cdot6'} & c_{0\cdot7'} & c_{0\cdot8'} & c_{0\cdot3'} & c_{0\cdot4'} & c_{0\cdot5'} & c_{0\cdot0'} & c_{0\cdot1'} & c_{0\cdot2'} \\ c_{0\cdot6'} & \cdot & \cdot & \cdot & \cdot & \cdot & \cdot & \cdot & \cdot \\ c_{2\cdot6'} & & \cdot & & & & & & \cdot \\ c_{3\cdot6'} & & & \cdot & & & & & \cdot \\ c_{4\cdot6'} & & & & \cdot & & & & \cdot \\ \cdot & & & & & \cdot & & & \cdot \\ \cdot & & & & & & \cdot & & \cdot \\ \cdot & & & & & & & \cdot & \cdot \\ c_{8\cdot6'} & c_{8\cdot7'} & c_{8\cdot8'} & \cdot & \cdot & \cdot & \cdot & \cdot & c_{8\cdot8'} \end{bmatrix}. \quad (10)$$

Figures 15–18 give the results for a 2×2 m square primary source situated 1 m above the ground at a microphone distance of 50 m. Two cases of ground condition are considered: (a) 100% reflecting surface similar to a hard solid surface such as concrete, and (b) 50% reflecting surface with 90° phase change at the surface representing softer porous surfaces. The figures are computed for 100

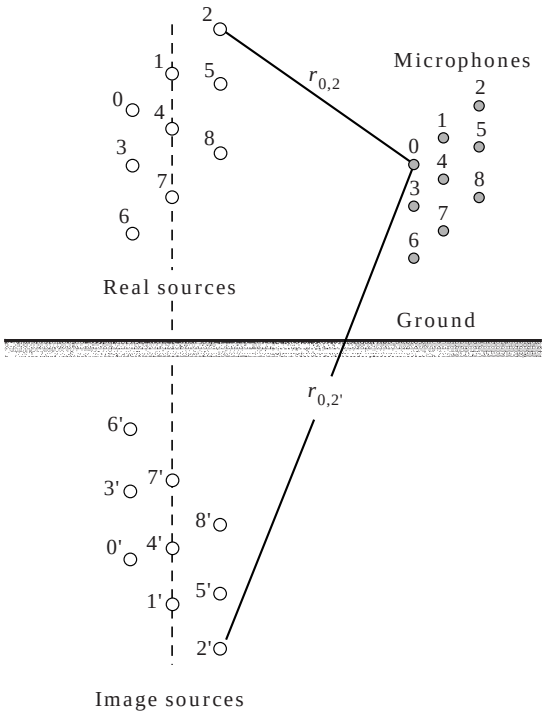

Figure 14. Array of point sound sources, images and microphones.

and 400 Hz source frequencies. Because of the ground plane, negative elevation angles ($-0°$ to $-30°$) are physically not accessible.

For 100% ground reflection the maximum radiation, as is to be expected, is increased nearly twofold, from $\sim$95 to 99 dB compared with the free field case at $f = 100$ Hz (Figure 2(a)). At higher frequencies, non-compact source case, $f = 400$ Hz, the effect of the ground is to produce additional horizontal interference ridges (maxima and minima in elevation, vertical axis), compared to the freefield case, because the source is now effectively twice as high (real source plus image).

Although the directivities exhibit some change, it can be seen that for the particular geometry and frequencies used, the shadow depths (75 dB at 100 Hz and 45 dB at 400 Hz) are little affected by ground reflection. Although the reflected primary source is now effectively twice its free field size, the cancellers are also effectively twice as many. The net effect can be considered as a cancelled reflected shadow, not much different than the freefield version.

5. DIRECTIONAL SECONDARY SOURCES

A fourth simplification used in the basic ECAS model was to use monopole cancelling secondary sources. These sources radiate equally in all directions (omnidirectional). More realistic sources tend to be directional.

The previous sections have described the properties of monopole secondary sources which redistribute acoustic energy within control angles from the

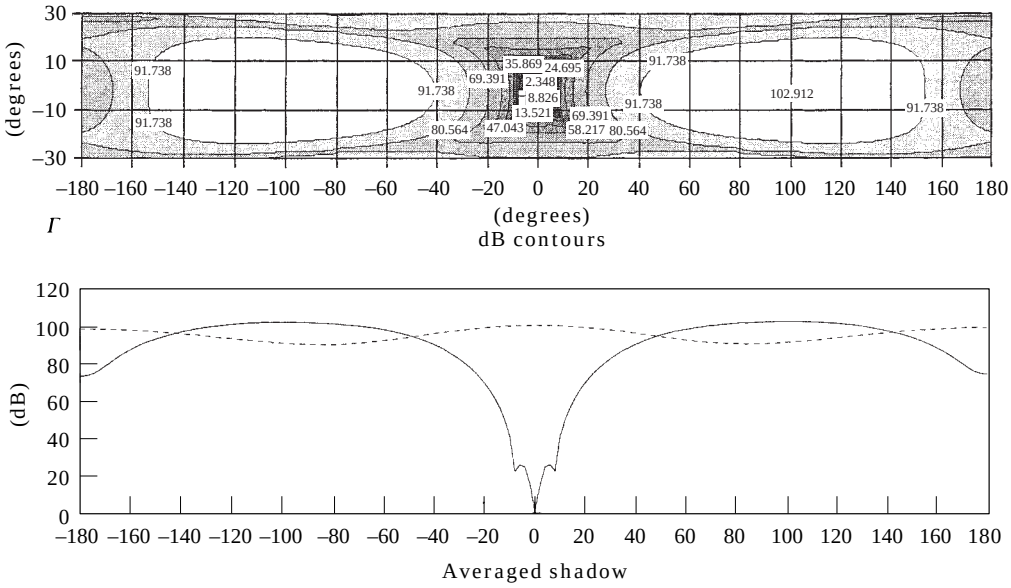

Figure 15. 100-Hz unit shadow with 100% ground reflecting surface (no change of phase).

primary source. Increases in sound outside these control angles can also be generated. This is because the monopole radiation is omnidirectional and uncoordinated there. A method of reducing this side radiation, and also radiation to the rear, is to use directional multiples.

The dipole, for example, has a figure of eight directivity: i.e., radiating equally, but out of phase, to the front and rear of its axis, but not radiating directly to the sides. A tripole (dipole plus monopole) has a heart shaped directivity along

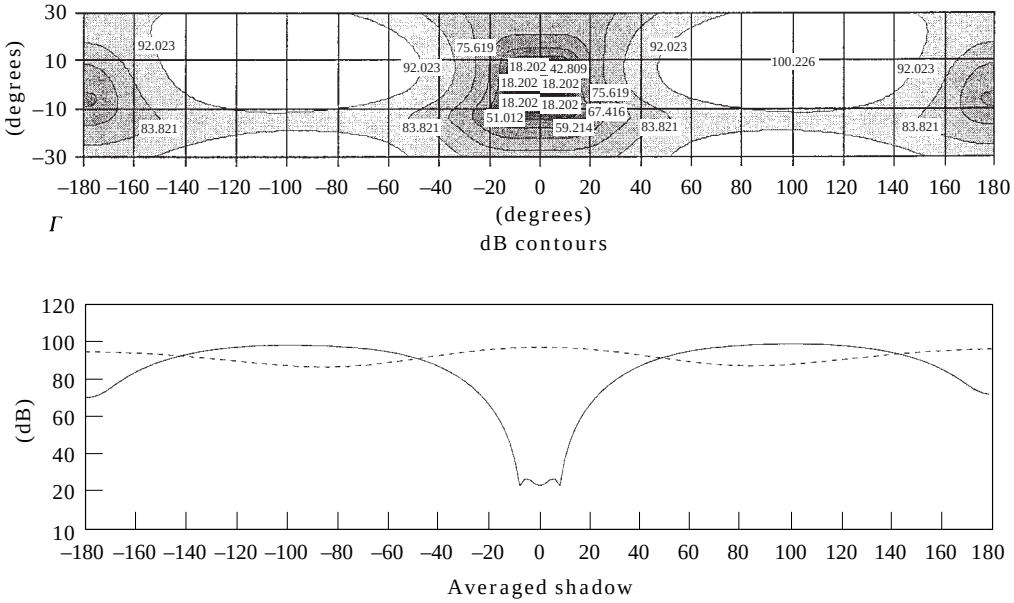

Figure 16. 100-Hz unit shadow with 50% ground reflecting surface (90° change of phase).

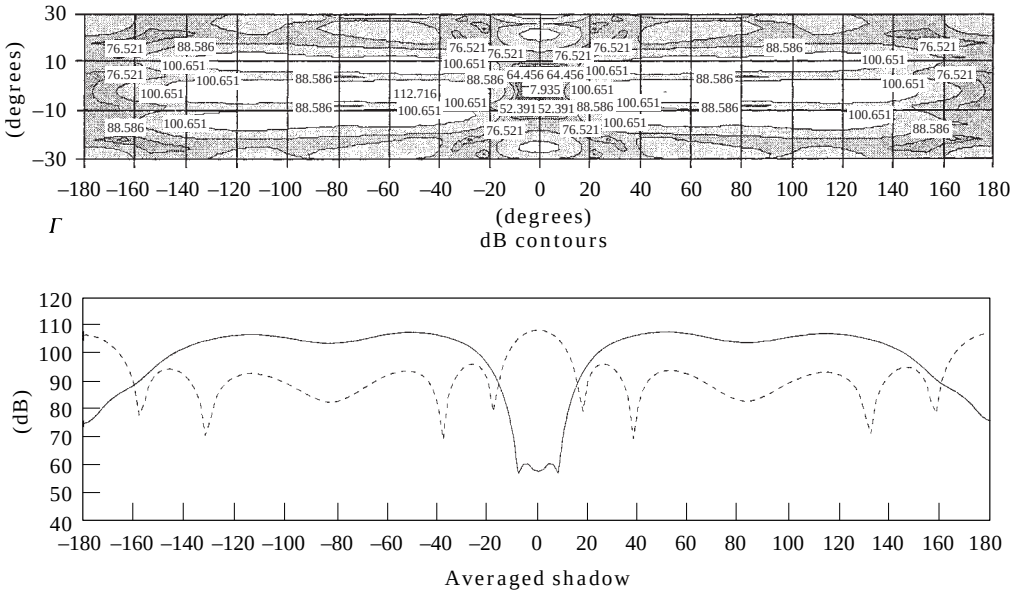

Figure 17. 400-Hz unit shadow with 100% ground reflecting surface (no change of phase).

its axis, radiating a maximum in front and progressively less moving to the rear. This has an important net forward energy propagating characteristic which can be used to represent a Huygens' propagating wave front. Tripoles, in principle, can thus be used to cancel (absorb) another propagating wave moving in the same direction without redirecting the energy (reflection).

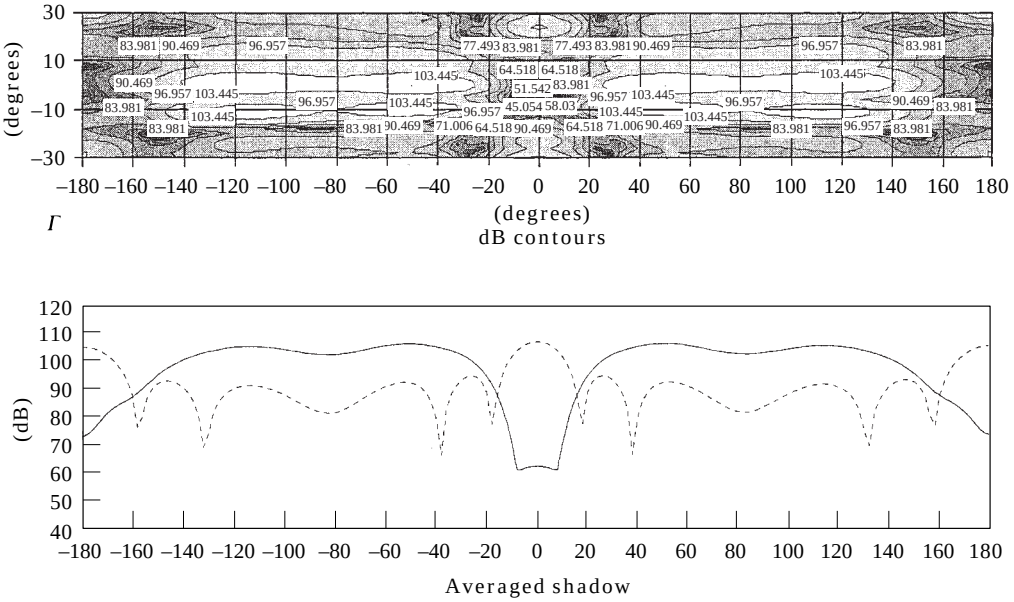

Figure 18. 400-Hz unit shadow with 50% ground reflecting surface (90° change of phase).

5.1. BASIC MONOPOLE

The ideal point monopole source is usually explained using the concept of a pulsating sphere which radiates sound equally in all directions, from equations (4) and (5) one has

$$p(r) = \mathrm{j}\omega\rho_0 q\, \mathrm{e}^{-\mathrm{j}kr}/4\pi, \tag{11}$$

where the quantities are defined after equation (5).

5.2. DIPOLE

The dipole source can be formed using two monopole sources, as illustrated in Figure 19, with strengths q_1 and q_2 of equal magnitude and opposite phase, and propagating distances r_1 and r_2, respectively, such that

$$p(r, \theta) = \frac{\mathrm{j}\omega\rho_0 q}{4\pi}\left(\frac{\mathrm{e}^{-\mathrm{j}kr_1}}{r_1} - \frac{\mathrm{e}^{-\mathrm{j}kr_2}}{r_2}\right). \tag{12}$$

If the separation distance between the sources is d, then in the far field ($kr \gg 1$), $r \gg \lambda/2\pi$, the approximation $r_1 \approx r_2 \approx r$ can be made in the denominator and $r_1 = r - (d/2)\cos\theta$, $r_2 = r + (d/2)\cos\theta$ in the numerator. For a compact dipole source ($kd < 1$) $d < \lambda/2\pi$, equation (12) becomes, upon using $\mathrm{e}^{\mathrm{i}x} - \mathrm{e}^{-\mathrm{i}x} = 2\mathrm{j}\sin x \approx \mathrm{j}kd\cos\theta$,

$$p(r, \theta) = \frac{\mathrm{j}\omega\rho_0 q}{4\pi r}\, \mathrm{e}^{-\mathrm{j}kr}(\mathrm{e}^{\mathrm{j}kd\cos\theta/2} - \mathrm{e}^{-\mathrm{j}kd\cos\theta/2}) = -\frac{\omega\rho_0 q}{4\pi r}\mathrm{e}^{-\mathrm{j}kr}kd\cos\theta. \tag{13, 14}$$

Or retaining near field terms ($kr < 1$) this becomes

$$p_d = -\frac{\mathrm{j}\omega\rho_0 q}{4\pi r}\mathrm{e}^{-\mathrm{j}kr}kd(\cos\theta)(1 + 1/\mathrm{j}kr) : \tag{15}$$

i.e., the maximum dipole strength is a factor kd weaker than the monopole strength in the far field ($kr \gg 1$).

5.3. TRIPOLE

Adding one more monopole source at the centre of this dipole configuration, creates a tripole source, as shown in Figure 19. The strength q_c of this third monopole can be chosen to provide a minimum sound in the far field ($kr \gg 1$) to the left of the source combination: for example, making $p(r) \approx 0$ for $x \gg 0$. Since this pressure tends to zero, q_c can be found by solving the equation

$$p(r) = \frac{\mathrm{j}\omega\rho_0}{4\pi}\left(\frac{q\mathrm{e}^{-\mathrm{j}k(r+d/2)}}{r + d/2} - \frac{q\mathrm{e}^{-\mathrm{j}k(r-d/2)}}{r - d/2} + \frac{q_c\mathrm{e}^{-\mathrm{j}kr}}{r}\right) = 0. \tag{16}$$

Upon neglecting differences in the denominators, which is an acceptable approximation when working in the farfield region, the solution for q_c becomes

$$q_c = q(\mathrm{e}^{\mathrm{j}kd/2} - \mathrm{e}^{-\mathrm{j}kd/2}) = \mathrm{j}2q\sin(kd/2). \tag{17}$$

Again, for a compact tripole source ($kd < 1$) $q_c \approx \mathrm{j}qkd$, and for angles away from

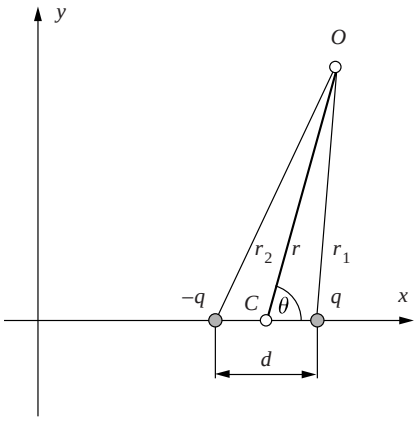

Figure 19. Classical multipole sources.

the x-axis substituting for $r_1 = r - (d/2)\cos\theta$, and $r_2 = r + (d/2)\cos\theta$, equation (16) in the far field ($kr \gg 1$), after some mathematical manipulation, simplifies to

$$p = \frac{-\omega\rho_0 q e^{-jkr}}{4\pi r} kd\{\cos\theta + 1\}. \tag{18}$$

The $\cos\theta$ term which has a dipole directivity, and the unity term which has a monopole directivity, together produce the tripole directivity.

5.4. PHASE CONTROLLED MULTIPOLES

The classical multipole sources considered above have a fixed phase between them, usually 180°. If the phase is adjusted with position and/or frequency, more efficient multipoles can result.

5.5. REFLECTING DIPOLE (TRIPOLE–DIPOLE)

Consider the farfield sound ($x \gg d$), right of two monopole sources labelled **1** and **2** shown in Figure 20. For simplicity the analysis is carried out in one dimension along the x-axis. Generally for off-axis sound, the on-axis distances will be modified by $\cos\theta$, where θ is the angle made with the x-axis. Further, the distance x in the denominator is considered to be similar for both poles, as in the far field. In this case the sound for $x \gg d$ becomes

$$p_{x>d} = p_1 + p_2 = (j\omega\rho_0/4\pi x)(q_1 e^{-jkx} + q_2 e^{-jk(x-d)}). \tag{19}$$

By adjusting the phase of source **2** with separation distance d from source **1** according to

$$q_2 = -q_1 e^{-jkd}, \tag{20}$$

the sound propagating to the right of source **2** will cancel: i.e.,

$$p_{x>d} = p_1 + p_2 \approx 0. \tag{21}$$

The sound propagating to the left of sources **2** ($0 < x < d$) will now be equal to the sound propagating to the right of source 1, and thus $p_2 = p_1$ ($x > 0$): i.e.,

source **2** acts not as a radiator but as a reflector, reflecting the sound from source **1** back to itself. The sound to the left of source **1** ($x \gg 0$), where x in the exponentials remains negative in the direction of propagation, is then

$$p_{x<0} = p_1 + p_2 = (\mathrm{j}\omega\rho_0/4\pi x)(q_1 \mathrm{e}^{-\mathrm{j}kx} + q_2 \mathrm{e}^{-\mathrm{j}k(x+d)}). \tag{22}$$

Using equation (20), one has

$$p_{x<0} = (\mathrm{j}\omega\rho_0/4\pi x) q_1 \mathrm{e}^{-\mathrm{j}kx}(1 - \mathrm{e}^{-\mathrm{j}2kd}) = (\mathrm{j}\omega\rho_0/4\pi x) q_1 \mathrm{e}^{-\mathrm{j}k(x+d)}(\mathrm{e}^{\mathrm{j}kd} - \mathrm{e}^{-\mathrm{j}kd})$$

$$= (-\omega\rho_0/4\pi x) q_1 \mathrm{e}^{-\mathrm{j}k(x+d)} 2\sin(kd). \tag{23}$$

Equation (23) gives the sound pressure, on-axis, to the left of the source combination. The sound to the right, in reality, will not be exactly zero. Its value will depend on the separation distance d between the sources. Its directivity is therefore that of a simulated tripole, as computed in Figure 21. The source strength q used in the computations is 1 m^3/s; the units in the figure are dBs and meters. This form of reflective dipole has the following properties: (a) a source strength of twice the monopole strength with maxima to the left when $\sin(kd) = 1$, $kd = \pi/2$, $d = \lambda/4$; (b) a much stronger source strength than the classical multipole, where the kdq direct multiplier source strength term in the classical multipole reduces the radiation, proportionally, for $kd < 1$: for example in the dipole equation (14) and the tripole equation (18); (c) the minima on the x-axis to the right ($x \gg d$) depends on the difference between the reciprocal distances from the monopole sources to the observer,

$$1/x - 1/(x + d) = d/x(x + d) \approx (d/x)1/x: \tag{24}$$

i.e., the inverse distance $1/x$ (spherical spreading) is modified by an additional (d/x) term, giving the minimum cancellation depth in dB as

$$\mathrm{dB} = -20\log(x/d); \tag{25}$$

thus the minima to maxima multipole value increases with distance from the source.

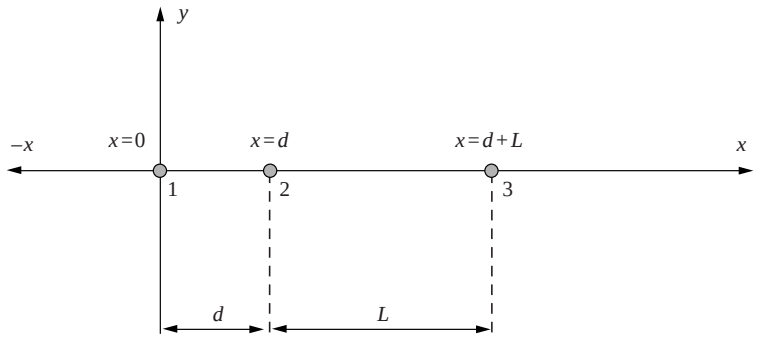

Figure 20. Phase controlled sources.

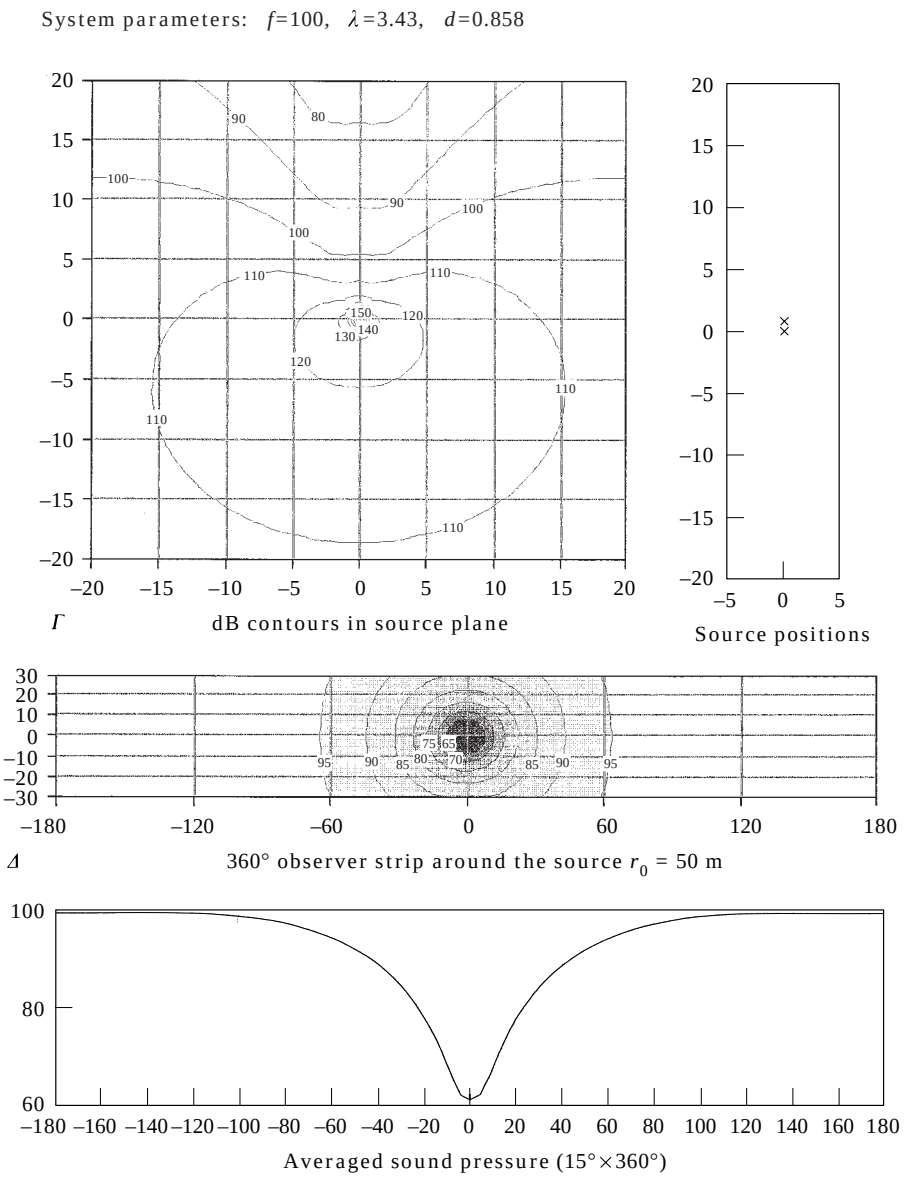

Figure 21. Phased multipole sources—reflective tripole dipole $d = \lambda/4$.

5.6. REFLECTING DIPOLE (RESONANT-DIPOLE)

For the special case of $kd = n\pi$, or $d = n(\lambda/2)$ where n is an integer, then $P_{x<0} \cong 0$, i.e., the sound to the left of the source combination will also cancel. Thus source 1 now acts as a reflector; the sound therefore reflects back and forth between sources 1 and 2, similar to a laser action. In this situation the tripole directivity is transformed into a dipole-like directivity. Here both sources are trying to cancel each other, producing a sharper elongated dipole directivity than the classical dipole, as shown in Figure 22. Note the minima along the dipole

axis are finite, have finite (wider) angle widths (not singularities as in the classical dipole case) and they are orthogonal to those of the classical dipole. Figure 23 shows a non-compact ($d > \lambda$) resonant dipole computed for $n = 4$, $d = 2\lambda$, which exhibits additional complex acoustic interference.

5.7. ABSORBING TRIPOLE

If now a third source **3** is introduced to the right of source **2** and separated by a distance L ($x = d + L$), as illustrated in Figure 20, then the sound propagating to the left of source **1** ($x \ll 0$) will become

$$p_{x<0} = p_1 + p_2 + p_3 = (\mathrm{j}\omega\rho_0/4\pi x)(q_1 \mathrm{e}^{-\mathrm{j}k(x+d)} 2\mathrm{j}\sin(kd) + q_3 \mathrm{e}^{-\mathrm{j}k(x+L+d)}). \quad (26)$$

If q_3 is adjusted now according to

$$q_3 = -q_1 \mathrm{e}^{\mathrm{j}kL} 2\mathrm{j}\sin(kd), \quad (27)$$

then the sound propagating to the left of source **1** will cancel, i.e., $P_{x<0} \cong 0$. Here, fascinatingly, the source pair **1** and **2** now absorb the sound from the left side of source **3** resulting in an absorbing form of tripole source.

As $p_2 = -p_1$ on the right side of sources 1 and 2 (from equation (21)), the sound to the right of source **3** ($x > d + L$), is given now by P_3 only: i.e.,

$$P_{x>d+L} = P_3 = (\mathrm{j}\omega\rho_0/4\pi x) q_3 \mathrm{e}^{-\mathrm{j}k(x-(d+L))}. \quad (28)$$

Substituting q_3 from equation (27) into equation (28) finally gives the sound pressure for the absorbing tripole as

$$P_{x>d+L} = (\omega\rho_0/4\pi x) q_1 \mathrm{e}^{-\mathrm{j}k(x-(d+2L))} 2\sin(kd). \quad (29)$$

This equation is identical to equation (23) for the reflecting dipole, apart from the minus sign and the additional exponential phase terms. These additional directional terms can be used to modify the directivity off-axis. However, the dominant term on-axis to the right of the three-source combination is $\sin(kd)$, giving properties similar to those of the reflecting dipole, except the maxima and minima are interchanged. Figure 24 shows the absorbing tripole form for $d = n(\lambda/4)$, for $n = 1$, and $L = \lambda/4$.

The dipole form of the three-source combination occurs for $d = n(\lambda/2)$, where the radiation on-axis and in the far field, is now independent of the value of L, for integer values of n, as $q_3 = 0$. This form is therefore equivalent to the reflecting resonant dipole directivity shown in Figure 22. Figure 25 shows the "almost" dipole form, for a close integer of n ($n \approx 2$) $d = 1{\cdot}6$ ($d \approx \lambda/2$). Here the radiation is now dependent on L. Additional poles can be added *ad infinitum*, producing a whole family of directivities.

These multipole sources make an interesting array of directional sources for focused sound cancellation systems, if needed. Further background information regarding multipole sources can be found for example in references [5–7].

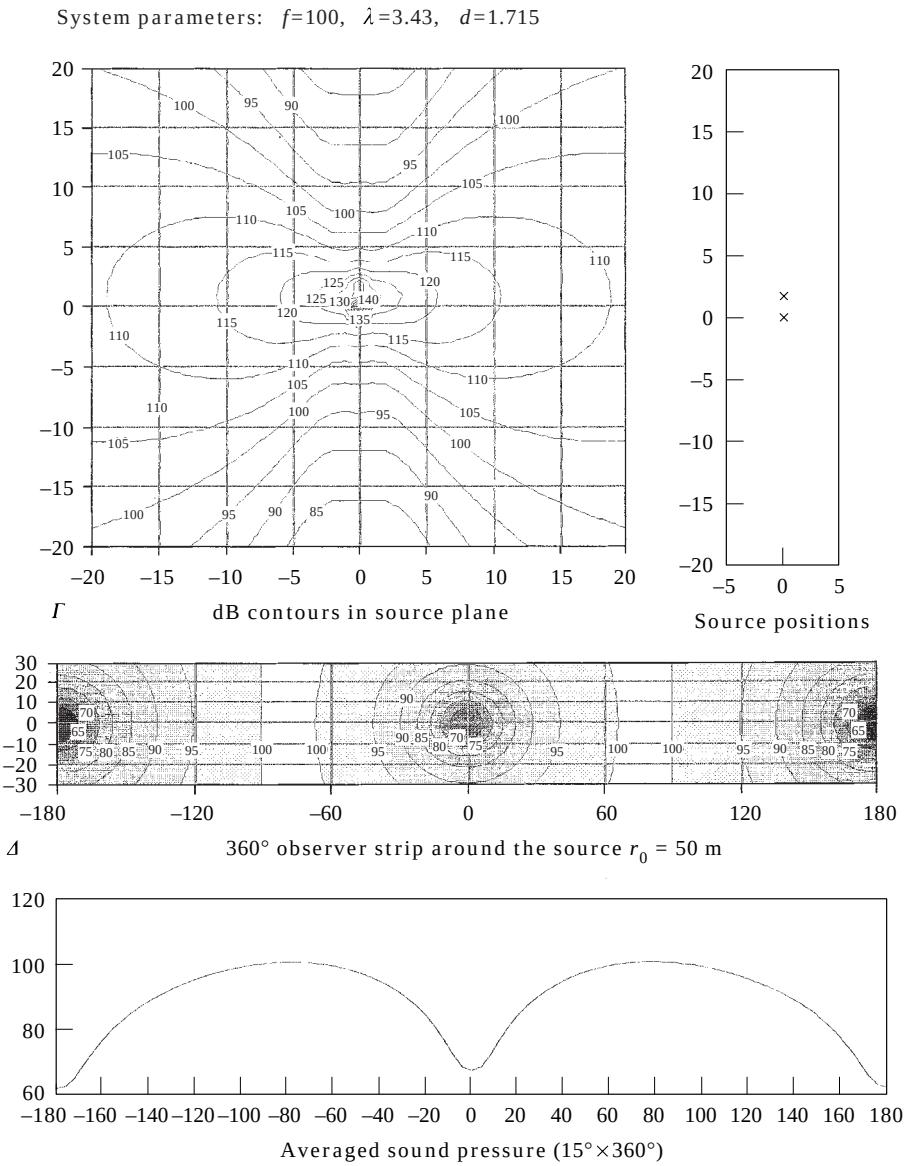

Figure 22. Phased multipole sources—reflective resonant dipole $d = \lambda/2$.

6. CANCELLING SYSTEMS

To return now to cancelling systems, the propagation elements of the matrices in the general case given by equation (9) contain transfer coefficients between each point secondary source and each microphone in the sensor area. These will be, for example, the monopole

$$c_{sm} = \omega\rho_0 \mathrm{e}^{-\mathrm{j}kr_{s,m}}/4\pi r_{s,m}, \tag{30}$$

the dipole

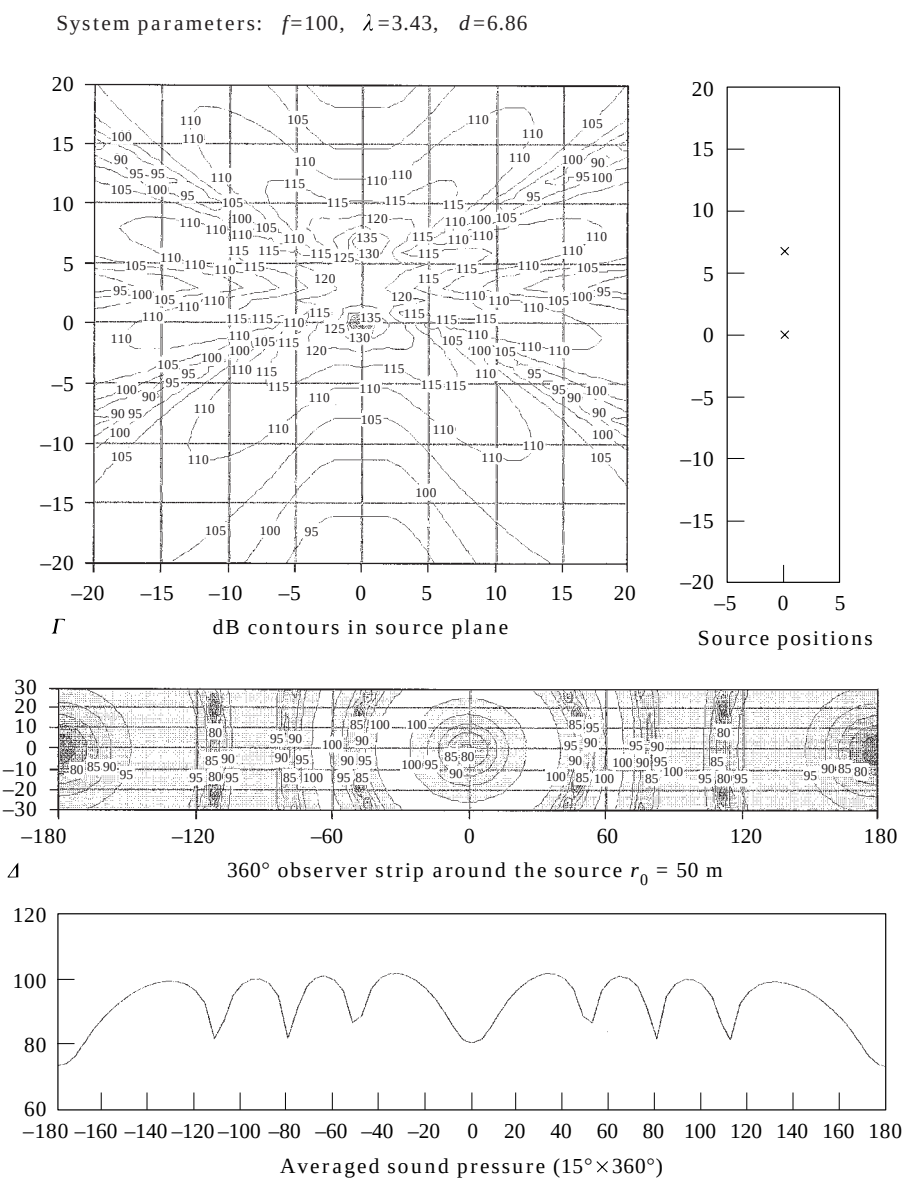

Figure 23. Phased multipole sources—reflective resonant dipole $d = 2\lambda$.

$$c_{sm} = \frac{\mathrm{j}\omega\rho_0}{4\pi}\left(\frac{\mathrm{e}^{-\mathrm{j}kr_{s,m}}}{r_{1_{s,m}}} - \frac{\mathrm{e}^{-\mathrm{j}kr_{s,m}}}{r_{2_{s,m}}}\right), \tag{31}$$

or, upon using its approximate compact ($kd < 1$) and far field ($kr \gg 1$), equivalent ($r_{1_{s,m}} \approx r_{2_{s,m}} \approx r_{s,m}$)

$$c_{sm} = -\frac{\omega\rho_0 \mathrm{e}^{-\mathrm{j}kr_{s,m}}}{4\pi r_{s,m}}(kd\cos\theta)\left(1 + \frac{1}{\mathrm{j}kr_{s,m}}\right). \tag{32}$$

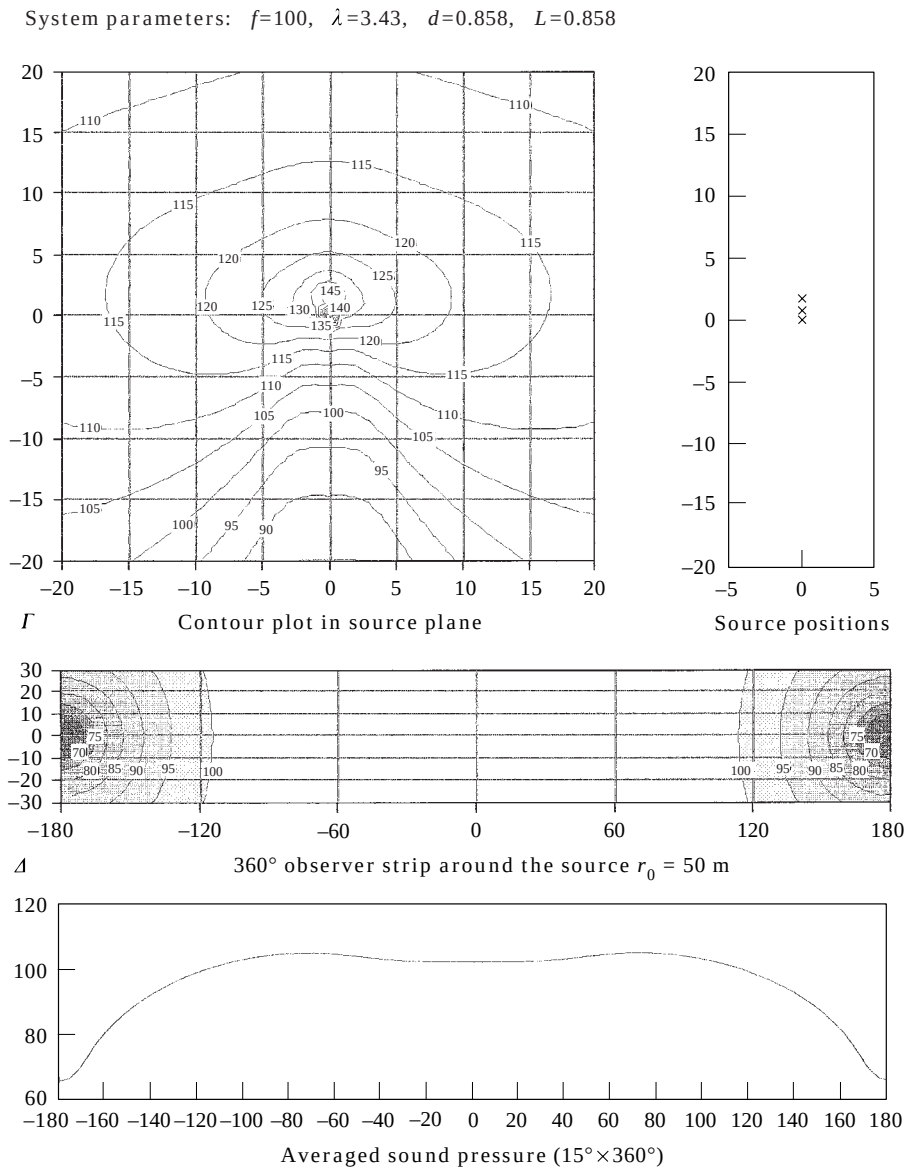

Figure 24. Phased multipole sources—absorbing tripole $d = \lambda/4$, $L = \lambda/4$.

For the tripole

$$c_{sm} = \frac{j\omega\rho_0}{4P}\left(\frac{e^{-jkr_{s,m}}}{r_{1_{s,m}}} - \frac{e^{-jkr_{s,m}}}{r_{2_{s,m}}} + K\frac{e^{-jkr_{s,m}}}{r_{s,m}}\right), \tag{33}$$

where $K = j2\sin(kd/2)$, or, upon using the approximate compact farfield form,

$$c_{sm} = (-\omega\rho_0/4\pi r_{sm})e^{-jkr}kd(\cos\theta + 1). \tag{34}$$

Incidentally, when working in a three-dimensional co-ordinate system the $kd\cos\theta$ part of the expression must be expanded to $kd\cos\theta\cos\varphi$ to include

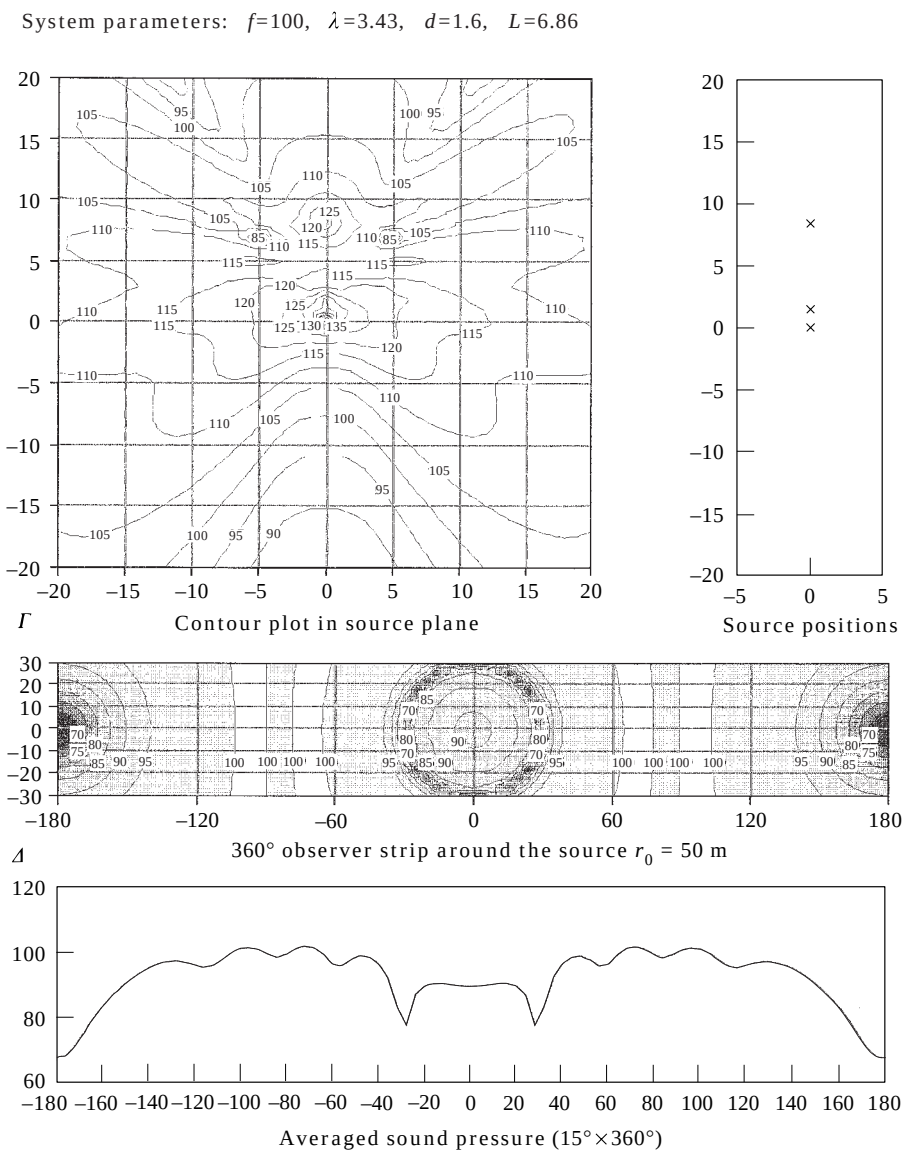

Figure 25. Phased multipole sources—absorbing tripole $d = 1{\cdot}6$, $L = 2\lambda$.

the influence of the elevation angle between each secondary source and microphone. These dipole and tripole secondary source system arrangements are shown in Figures 26 and 27. The exact equations (31) and (33) were used in the directional source computations, although the approximate equations (32) and (34) give almost identical results.

6.1. COMPUTED RESULTS

The first set of plots, Figure 28, represent the sound field in dB radiated normal to a wall of secondary sources *only* (no primary source present)

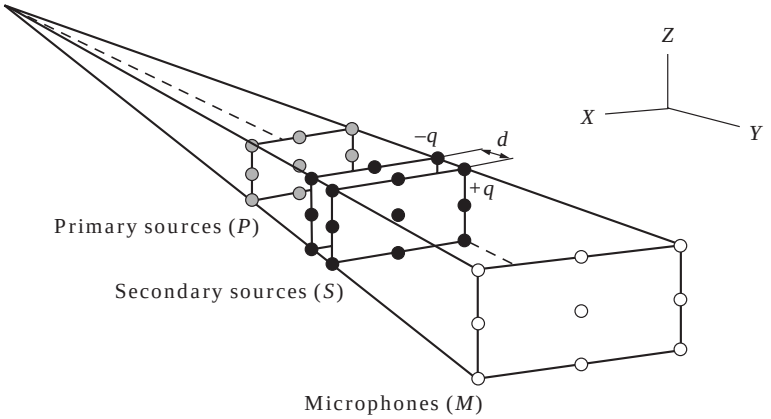

Figure 26. Secondary dipole source configuration.

calculated and plotted for the part of the plane $z = 0$ (60×60 m). Three different types of sources are, for example, simulated classical monopole (a), dipole (b) and tripole (c).

The 2×2 m square wall of secondary sources is created by using nine ideal, point monopole sources in a 3×3 arrangement. The dipole and tripole secondary source types for cases (b) and (c) are then created according to equations (31) and (33), as previously described, by adding one and two more layers of monopole sources. Separating distance between dipole layers is set to $d = 0{\cdot}1$ m.

According to equations (11), (15) and (18), the maximum effective source strengths are in successive order q, kdq, and $2kdq$. The elliptical shape of the contours, in the case of the 2D monopole source, is caused by marginal compactness of the 2-m square source, $\lambda/D = 1{\cdot}7$ ($D = 2$ m, $f = 100$ Hz). The other two plots for the classical dipole and tripole directivities, are for the same compactness factor.

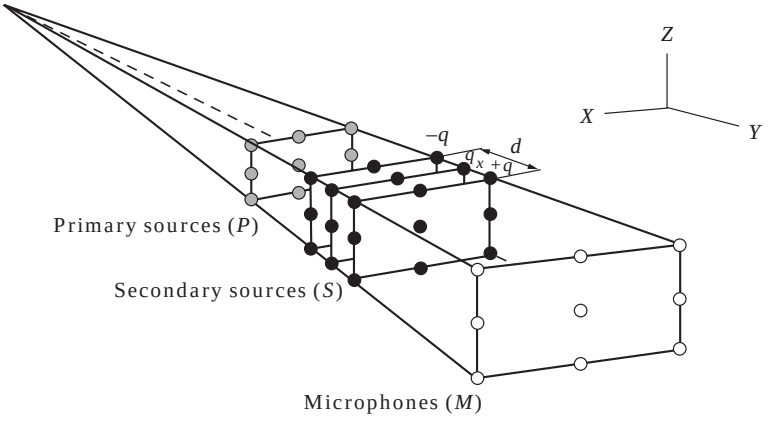

Figure 27. Secondary tripole source configuration.

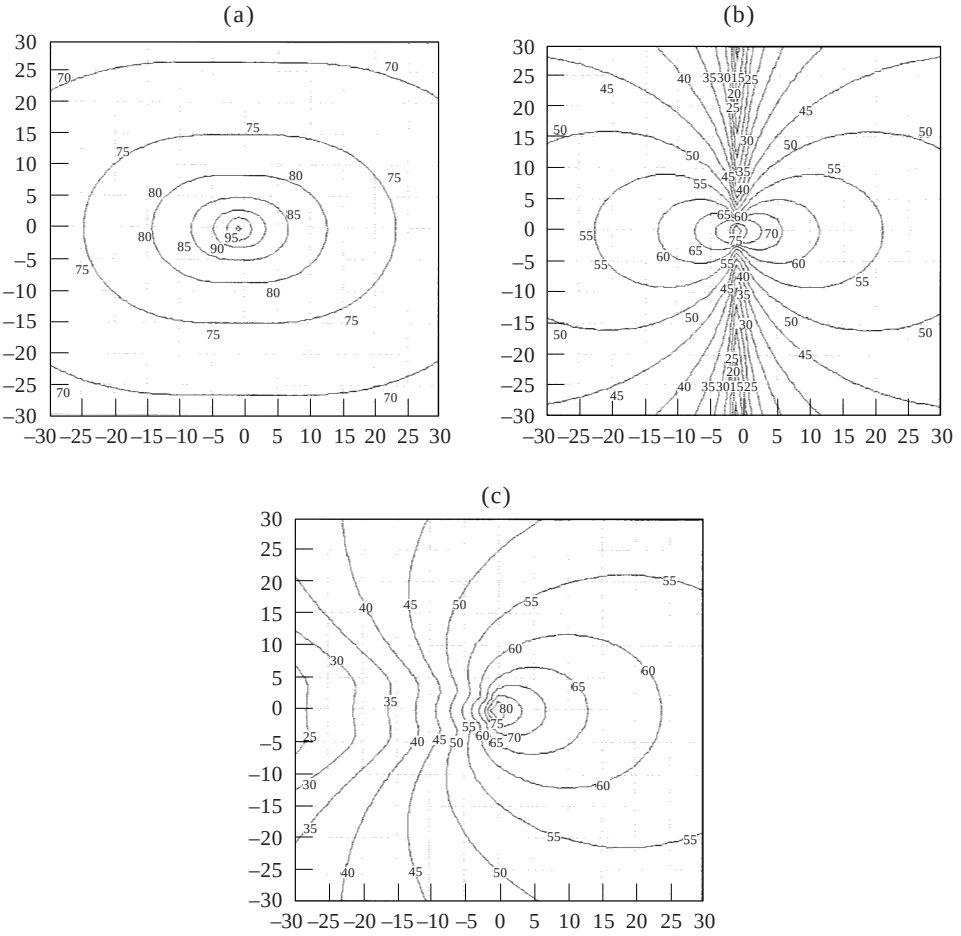

Figure 28. dB contours in xy plane ($z = 0$), generated by a wall of classical multipole sources: (a) monopole; (b) dipole; (c) tripole.

Figure 29 shows the computed shadows for the monopole (b), dipole (c) and tripole (d) secondary sources compared with the uncancelled field (a). The plots show $60 \times 360^\circ$ observer strips at an observer distance of $r_0 = 50$ m, for 100 and 400 Hz. In the case of the dipole secondary source, it can be seen that it is possible to reduce the increases in side radiation produced with the monopole source. The drawback is increased radiation behind the primary source.

Use of the tripole source, as expected, does not increase the radiation behind the primary source. Radiation immediately each side of the shadow (at high frequencies and for small shadow angles) is not reduced, but of course reduces progressively as the shadow angle increases towards 90°. Monopole and dipole source configurations with specific primary source–secondary source spacing ($r_s = \lambda/2$, for example) can also reduce the sound pressure behind the primary source, as well as in the shadow region.

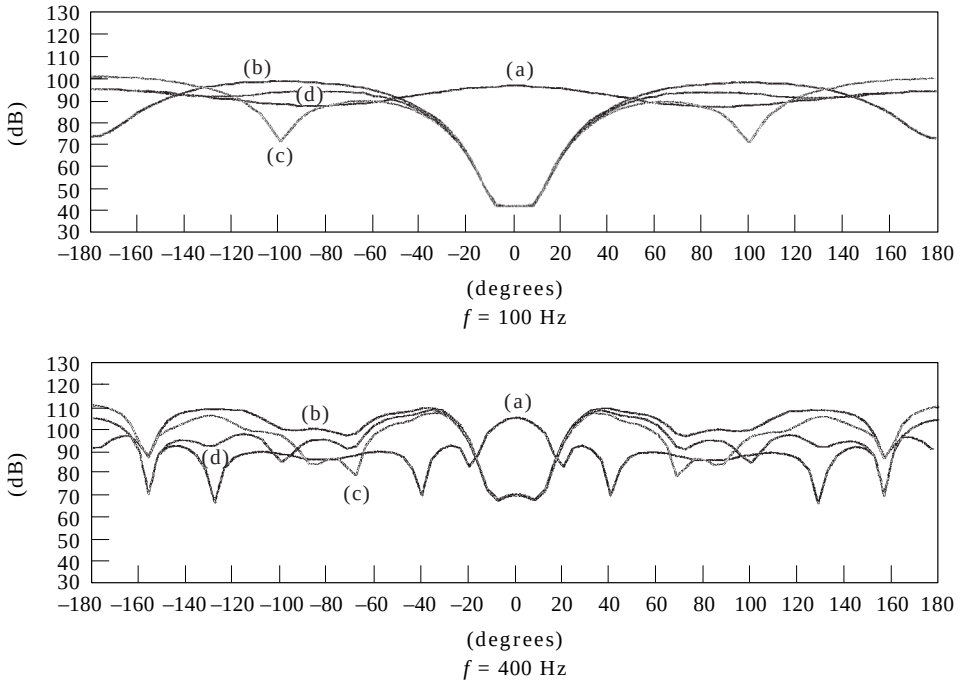

Figure 29. Multipole secondary source cancellation—averaged plots—summary, $r_0 = 50$ m: (a) uncancelled; (b) monopole; (c) dipole; (d) tripole.

The obvious example of a classical tripole type source is a loudspeaker backed by an absorbent enclosure behind, providing that the loudspeaker dimensions are small enough in comparison with the sound wavelength. The dipole source type can be realized by removing the backing enclosure of the loudspeaker since the sound produced in front of the loudspeaker and on the back are 180° out of phase. One of the practical problems with these kind of conventional multipole sources is their reduced source strength (kd) for the same q. Phased controlled multipole sources, which have been explored in section 5, seem to offer a better prospect for practical directional sound sources. These sources need to be investigated further.

7. WIND EFFECT

A fifth modification to the basically static ECAS model, is the effect of wind: i.e., the propagating fluid convecting across the stationary ECAS system.

Consider an acoustic wave propagating along a ray in a propagating fluid, again neglecting the harmonic time modulation term $\exp(j\omega t)$. The sound pressure at any point along the ray at a distance x from the sound source (positioned at $x = 0$) can be calculated from the solution of the one-dimensional wave equation as

$$p(x) = \mathrm{j}\omega\rho q \mathrm{e}^{-\mathrm{j}kx}/4\pi x, \quad k = \omega/c. \tag{35}$$

The symbols are the same as those defined after equation (5).

In the early days, there appeared to be confusion regarding the development of the convected wave equation. The initial work in this area was in the development of the "convected" electromagnetic wave equation (space travel, Einstein *et al.*). The confusion resulted from trying to derive the acoustic equation from the electromagnetic one, where of course there is no propagating medium, in the classical sense. Providing it is kept in mind that equation (35) describes the fundamental wave propagation physics of sound propagation with respect to a propagating medium, then there is no confusion.

The effect of wind (sound propagation in the propagating medium moving with a speed u' with respect to a stationary reference frame—ground), can be found now by modifying the quantities in equation (35) by those observed from the ground frame. All symbols in the moving frame, where the actual wave propagation occurs with respect to that frame, will be plain. All symbols in the stationary ground frame, where the apparent wave propagation is being observed, will be denoted by a superscript. Thus, the new speed of sound c' with respect to the stationary co-ordinate axis x', can now be obtained by using a simple vector superposition principle. Adding the two vectors—wind speed velocity u' with respect to the ground and the sound propagation velocity in the medium c, gives the new sound velocity c' with respect to the ground as

$$\left\{ \begin{array}{ll} c' = c + u' & \text{for the same direction of both velocity vectors} \\ c' = c - u' & \text{for the opposite direction of sound and wind speed} \end{array} \right\}. \tag{36}$$

Generally

$$c' = c(1 \pm u'/c) = c(1 \pm M'), \tag{37}$$

where M' is the Mach number,

$$M' = u'/c. \tag{38}$$

Now x in equation (35) is the actual propagation distance in the propagating fluid; it is used to describe waves propagating with velocity c, to P, in the propagation time $t_p = x/c$. x' is the apparent propagation distance, as measured in the stationary frame, with waves moving to point P' with effective velocity c', in the same propagation time t_p. By the time the actual sound has propagated to point P, P has moved on a distance d' to coincide with P', as measured in the stationary (ground) frame, as illustrated in Figure 30.

As the propagation time in both frames is the same, then

$$t_p = x/c = x'/c', \quad x' = x\left(\frac{c + u'}{c}\right) = x(1 + M') \tag{39, 40}$$

and

$$d' = x' - x = x(1 + M') - x = xM'. \tag{41}$$

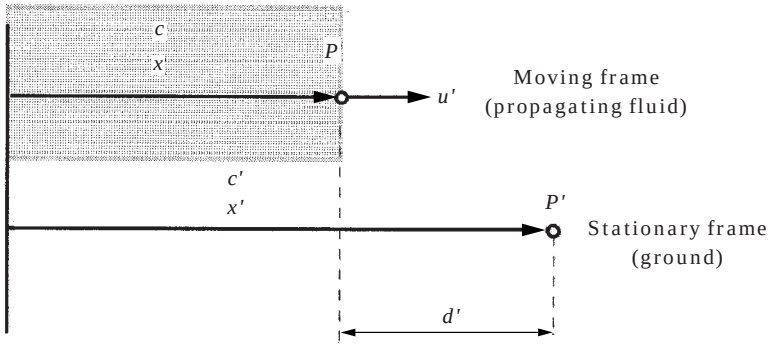

Figure 30. One dimension sound propagation with wind.

The effect of wind on the source strength q is not considered here. This effect is considered in more detail in reference [8]. For moderate wind speeds the effect is small.

The problem in two-dimensional space, where in general, the vectors c' and u' do not lie on the same line, requires the application of trigonometry as illustrated in Figure 31. Here, the actual propagation distance x is replaced by r in equation (35). This distance has to be defined in terms of quantities that are measured in the stationary frame (on the ground): i.e., r', d', M', and α'. Applying the cosine rule on the triangle OPP$'$ one has:

$$r^2 = r'^2 + d'^2 - 2r'd' \cos\alpha. \tag{42}$$

Generally $d' = rM'$ (two-dimensional equivalent of equation (41)) so one can rearrange equation (42) to obtain r as

$$r^2(1 - M'^2) + 2r'rM' \cos\alpha' - r'^2 = 0. \tag{43}$$

Solving for r yields:

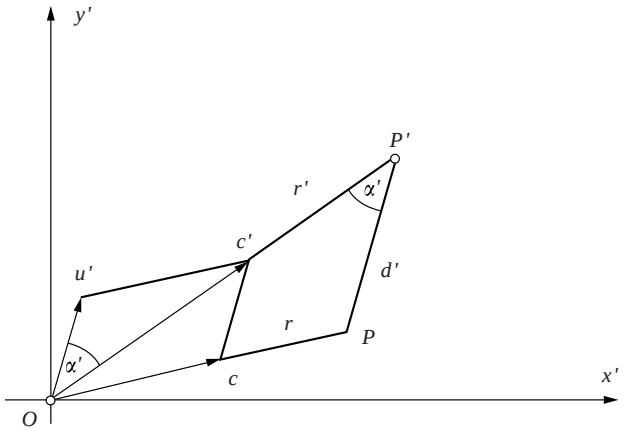

Figure 31. Two dimension sound propagation with wind.

$$r = \frac{-2r'M'\cos\alpha' \pm \sqrt{(2r'M'\cos\alpha')^2 - 4(1 - M'^2)r'^2}}{2(1 - M'^2)}, \tag{44}$$

or simply

$$r = \frac{r'}{1 - M'^2}(\pm\sqrt{1 - M'^2\sin^2\alpha'} - M'\cos\alpha'); \tag{45}$$

$$r = \frac{r'}{\sqrt{1 - M'^2}} \quad \text{if} \quad \alpha' = 90^\circ, \qquad \text{or} \qquad r = r'/1 + M' \quad \text{if} \quad \alpha' = 0^\circ. \tag{46a, b}$$

Equation (46a), for $\alpha' = 90^\circ$, is the Lorentz transform, or the Fitzgerald contraction, in the "convection" of electromagnetic waves. Equation (45) gives the required relation between the actual propagation distance r in the moving frame, and the apparent propagation distance r' in the stationary ground frame. The sound pressure at any fixed point on the ground can thus be calculated with wind, by substituting r from equation (45) for x in equation (35).

Figure 32 shows the sound field in dB over a 20×20 m square area radiated from a point monopole source for four different wind speeds (Mach numbers). It illustrates sound wave compression with increasing wind speed from, left to right, until a stationary supersonic wave front (boom) with respect to the ground is formed, for $M' > 1$. This is a trivial application, but it does validate the developed computer modelling for more complex cases, such as-non compact multipole source distributions with convected motion.

7.1. RESULTS

The effect on shadow performance has been simulated for wind conditions by using equation (45) incorporated into the basic ECAS model for the standard case shown in Figure 2. The results are summarized in Figure 33. All four figures show an average SPL in dB around the source (360°) for four different wind speeds: 50, 100, 200 and 300 m/s (using progressively lighter traces with wind speed in the figure). These speeds are unrealistically high to exaggerate the effect of wind. The wind direction was along the y-axis in the co-ordinate system shown in Figure 31.

Figure 33(a) summarizes the acoustic shadows at a microphone and observer distance of 50 m, with wind, but cancellers not optimized for wind condition. It can be seen that the lightest wind "blows away" the acoustic shadow and completely ruins the ANC system performance. The second set of acoustic shadows, Figure 33(b) shows the system performance under identical wind conditions, but now with self-optimization of the cancellers for wind conditions. The shadows, although reduced and somewhat distorted, appear to be adequately deep and still in place, even for excessive wind speeds. In this case the cancellers now automatically compensate for the wind direction, producing a net zero deflection of the shadow with observer distance. This is still true for an observer at 500 m, as demonstrated in Figure 33(c). Figure 33(d) shows the system performance at 50 m but at a higher frequency of $f = 400$ Hz.

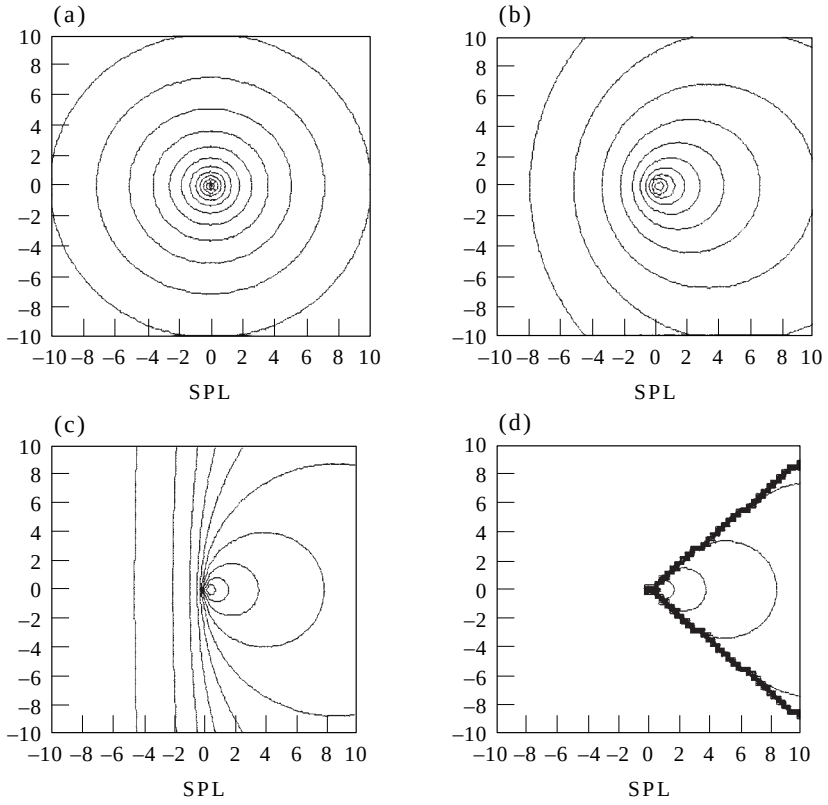

Figure 32. Radiation pattern for point monopole source and four wind speeds (varification of computation): (a) $M' = 0$; (b) $M' = 0{\cdot}5$; (c) $M' = 0{\cdot}99$; (d) $M' = 1{\cdot}5$.

These figures demonstrate a remarkable characteristic of ECAS systems; i.e., the ability of the secondary sources to adapt according to different wind speeds. This intelligence provides deep acoustic shadows, staying on course, even under high cross-wind and large propagation distances.

8. CONCLUSIONS

Practical extensions to the basic ECAS theory have been modelled. The results can be summarized as follows.

(a) Out of phase primary sources deteriorate shadow performance by about 25 dB, for compact sources, and about 20 dB for non-compact sources, compared with in-phase sources.

(b) Three-dimensional primary sources reduce the shadow performance by about 20 dB, for compact sources, and about 10 dB for non-compact sources, compared with two-dimensional sources.

(c) Ground reflection has little effect on overall shadow performance for the particular ECAS geometry and frequencies investigated.

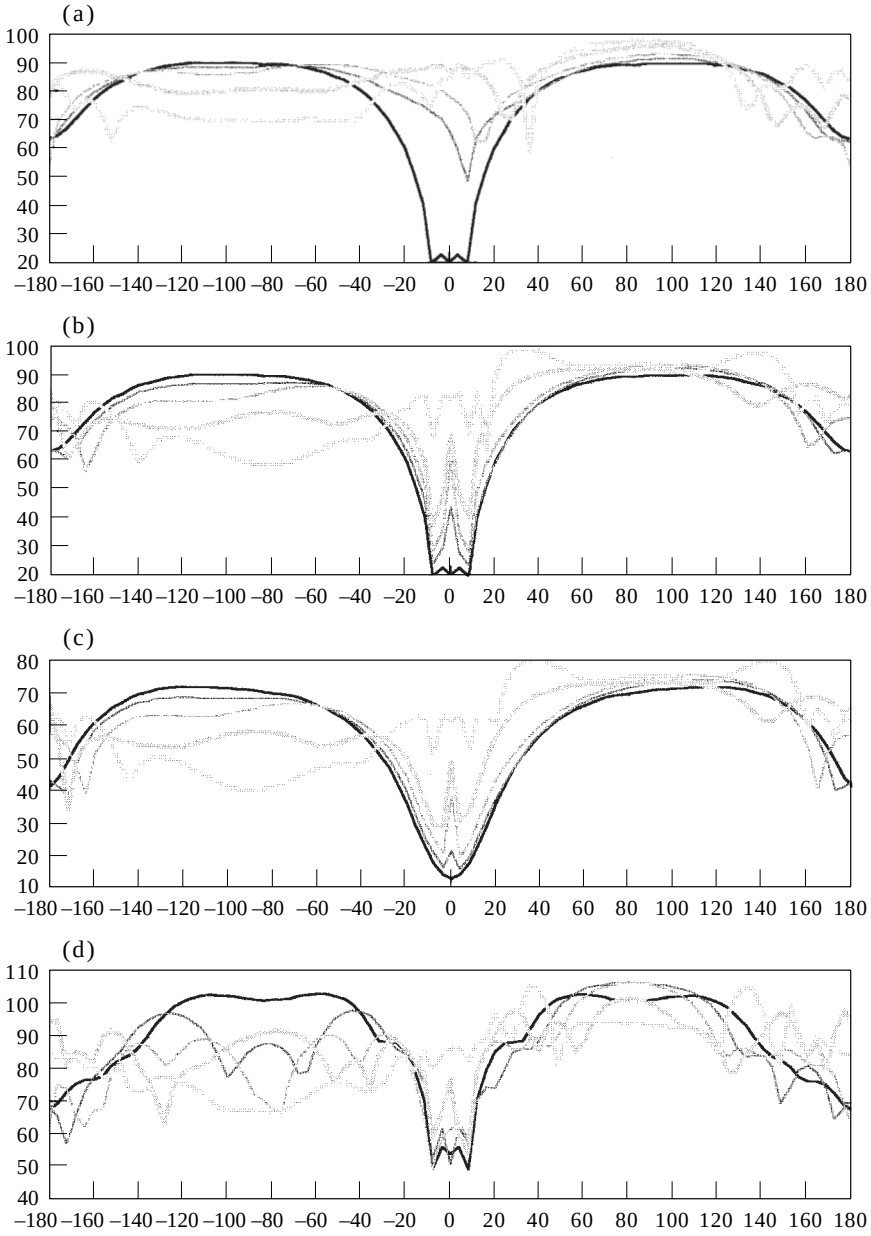

Figure 33. Averaged unit shadow in wind conditions: (a) no cancellation with cross wind, $f = 100$ Hz; (b) cancellation with cross wind, $f = 100$ Hz; (c) cancellation with cross wind, greater observer distance ($r_0 = 500$ m), $f = 100$ Hz; (d) cancellation with cross wind conditions, $f = 400$ Hz.

(d) Multipole directional secondary sources can absorb sound (without energy redirection), thus reducing unnecessary radiation to the side of the shadow. A fascinating family of phased multipole sources are identified which could be used to produce these focusing properties, if needed.

(e) It is found that the intelligence of the cancelling system has the remarkable ability to compensate for the effect of cross wind on cancellation performance. Even for strong winds the effect on shadow performance is small.

(f) If the above effects are multiplicative (dB addition), the worst case situation corresponds to about 55 dB shadow deterioration.

(g) Since shadow depths >120 dB are theoretically possible with ECAS systems, practical shadows >20 dB should be readily achievable with practical systems.

(h) Active noise control in unrestricted space with its progressive field has the potential to produce deep shadows over large distances.

REFERENCES

1. S. E. WRIGHT and B. VUKSANOVIC 1996 *Journal of Sound and Vibration* **190**, 565–585. Active control of environmental noise, I.
2. S. E. WRIGHT and B. VUKSANOVIC 1997 *Journal of Sound and Vibration* **202**, 313–359. Active control of environmental noise, II: non-compact acoustic sources.
3. S. E. WRIGHT and B. VUKSANOVIC 1999 *Journal of Sound and Vibration* **220**, 469–496. Active control of environmental noise, III: implementation of theory into practice.
4. L. E. KINSLER, 1982 *Fundamentals of Acoustics* New York: John Wiley & Sons; second edition. See pp. 78–82.
5. P. E. DOAK 1965 *Proceedings of the Fifth International Congress on Acoustics*, *Liège*, *Paper K*56. Multipole analysis of acoustic radiation.
6. M. A. SWINBANKS 1973 *Journal of Sound and Vibration* **27**, 411–436. The active control of sound propagation in long ducts.
7. P. A. NELSON and S. J. ELLIOTT 1993 *Active Control of Sound*. London: Academic Press.
8. S. E. WRIGHT 1986 *Journal of Sound and Vibration* **108**, 361–378. Sources and observers in motion, I: time variant analysis and its implications for aerodynamic sound.